Predicting Subseismic Fracture Density and Orientation in the Gorm Field, Danish North Sea: An Approach Using Elastic Dislocation Models*

Brett Freeman[1], David Quinn[1], Cathal G. Dillon[1], Michael Arnhild[2], and Bastiaan Jaarsma[3]

Search and Discovery Article #20321 (2015)**
Posted September 21, 2015

*Adapted from oral presentation given at AAPG 2015 Annual Convention and Exhibition, Denver, Colorado, May 31 – June 3, 2015

[1]Badley Geoscience Ltd, Hundleby, United Kingdom (Brett@badleys.co.uk)
[2]Maersk Oil Norway AS, Stavanger, Norway
[3]EBN, Utrecht, Netherlands

Abstract

The chalk reservoir of the Gorm field, southern North Sea is dome shaped and faulted due to a combination of salt diapirism and regional E-W extension. Fractures developed in the structure considerably enhance permeability. The dataset discussed here records fractures in horizontal wells from more than 10km of image logs and provides a special opportunity to test theoretical models of fracture development with quantitative observations. In an effort to forecast fracture density and fracture orientation we have estimated the strains in the structure using an elastic dislocation model that incorporates mechanical boundaries in the form of the tectono-stratigraphic interface with salt and tectonic faults. More than 50% of the angular differences between poles to the planes of simulated and observed fractures are less than 30 degrees, 75% are less than 45 degrees. Relative strain magnitude appears to be a useful indicator of fracture density. At the field scale, small strain magnitudes correspond with small non-zero fracture densities and relatively large strain magnitudes correspond with high fracture densities.

Reference Cited

Esmerode, E.V., H. Lykke-Andersen, and F. Surlyk, 2008, Interaction between bottom currents and slope failure in the Late Cretaceous of the southern Danish Central Graben, North Sea: Journal of the Geological Society, v. 165, p. 55–72.

Predicting subseismic fracture density and orientation in the Gorm Field, Danish North Sea: an approach using elastic dislocation models

Brett Freeman, David Quinn, Cathal Dillon (Badleys)

Michael Arnhild (Maersk)

Bastiaan Jaarsma (EBN)

Acknowledgements

Location

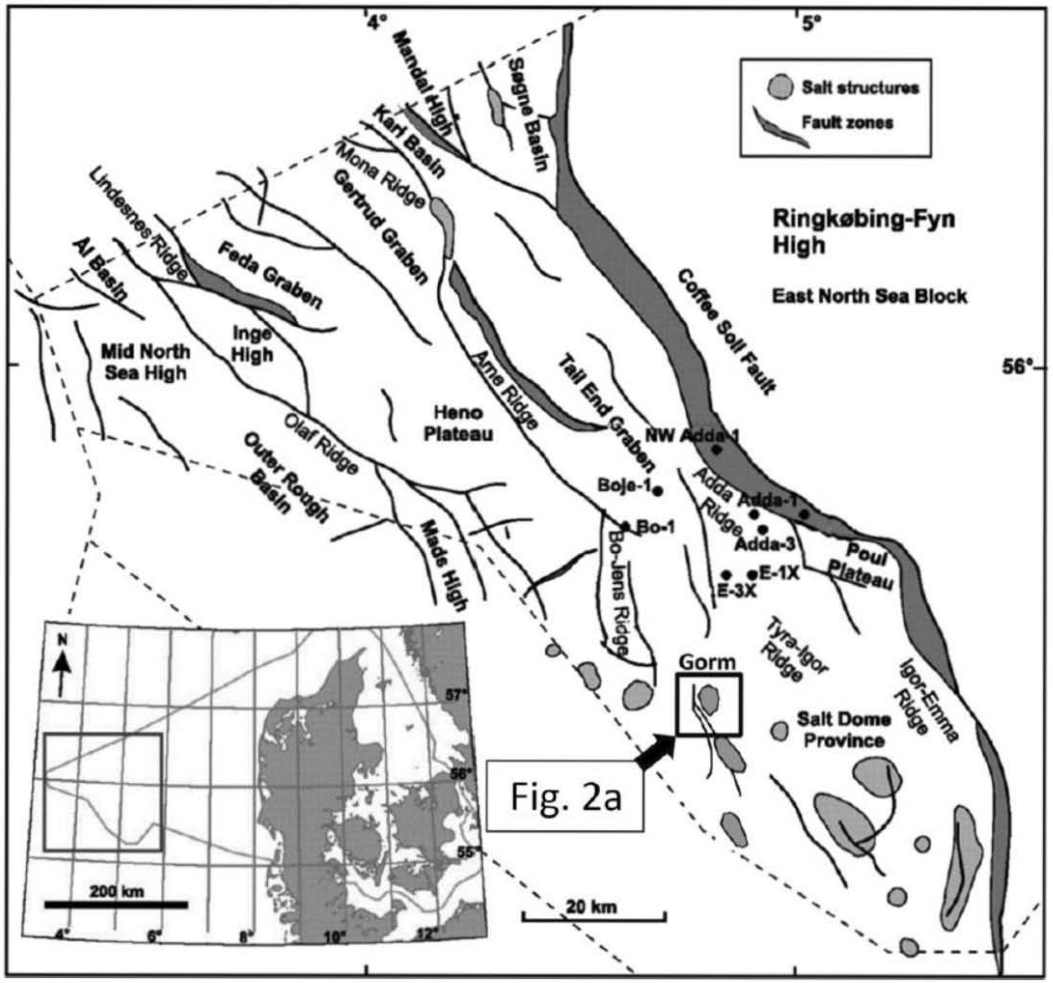

Fig. 1. Jurassic elements of the Danish Central Graben after Esmerode *et al.* (2008). The bold square marked 'Fig. 2a' indicates the location of the Gorm Field.

Setting

- Chalk field, operated by Maersk, Producing since 1981, 327 mb oil, 580 bscf gas
- Zechstein salt (seated at 5500 m - 7500 m) penetrates Jurassic rocks, present day top at 2750 m, 250 m beneath the base of the Chalk
- The Chalk thickness is approx. 500 m but is thinned on the crest in the form of a dome, present day top of the dome at approx. 1800 m
- Matrix permeability 0.5 mD - 8 mD, matrix porosity 15% - 45%
- Production is known to depend on fracture permeability

Available data

- More than 111 wells, 13 of which have in total more than 10 km image logs
- More than 16,000 logged fractures
- 433 fractures are considered to be large, sub-seismic shear fractures (i.e. faults) with observed offsets
- Density of these fractures up to 0.22 per m (approx. 1 every 5 m)
- 3D seismic data from 1998 and 2005 (time migrated and depth converted)
- Interpretation of seismically resolved faults (down to a min offset of about 20m)
- Interpretation of chalk reservoir boundaries, salt top and underlying basement

Objectives

- In any situation we run an ED model but we don't often get the opportunity to test the results so completely. Given the relative abundance of structural and fracture data, the Gorm field would appear to be an excellent natural laboratory.

- Using routinely available (depth converted) seismic interpretation and an Elastic Dislocation (ED) based continuum model which embodies deformation associated with the mechanical boundary between salt and overburden and mechanical interaction of coeval faults, can we make reasonable estimates of

- (a) sub-seismic fracture density

- (b) orientations of those fractures

Summary map and section

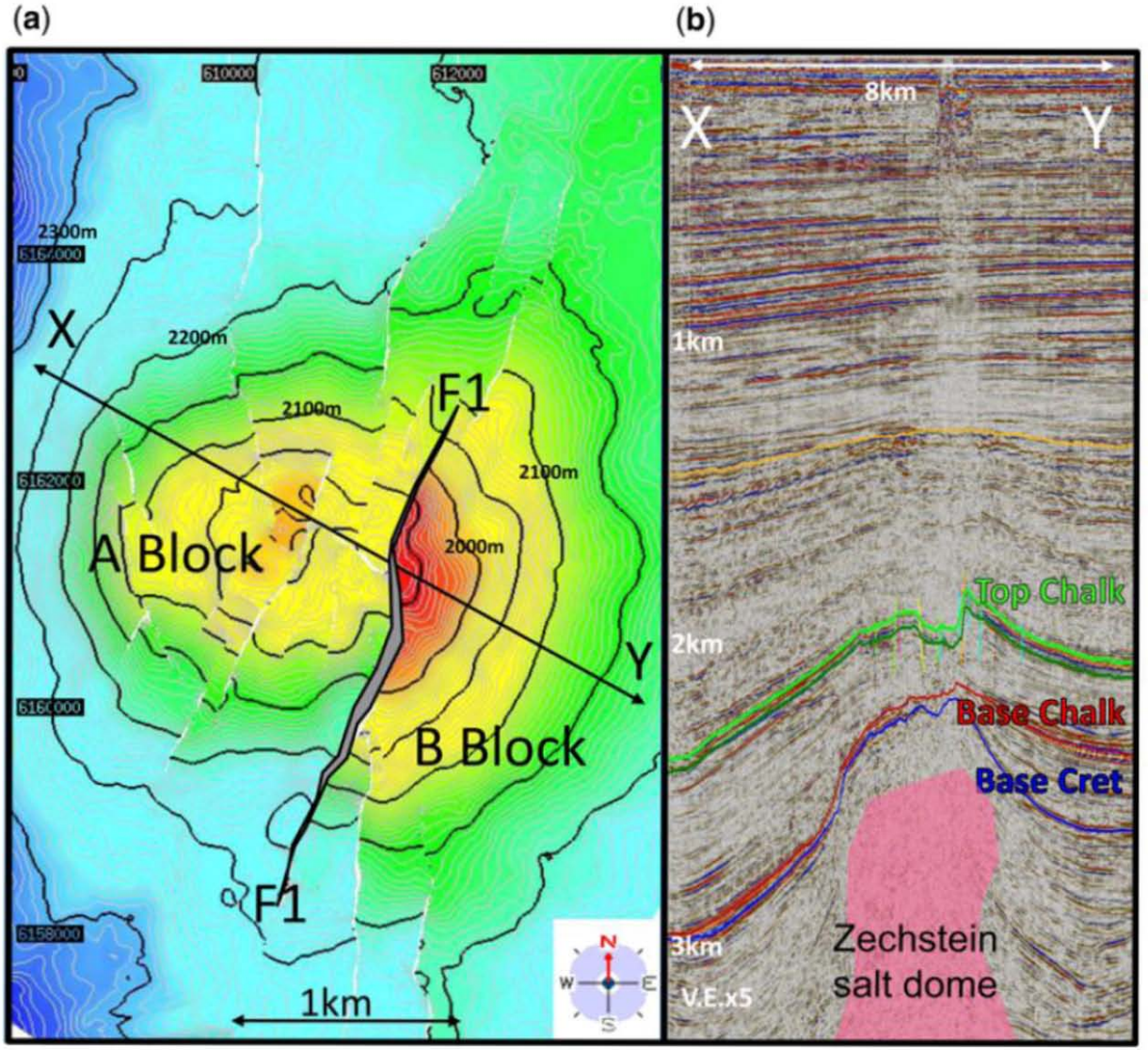

Structure of the faults

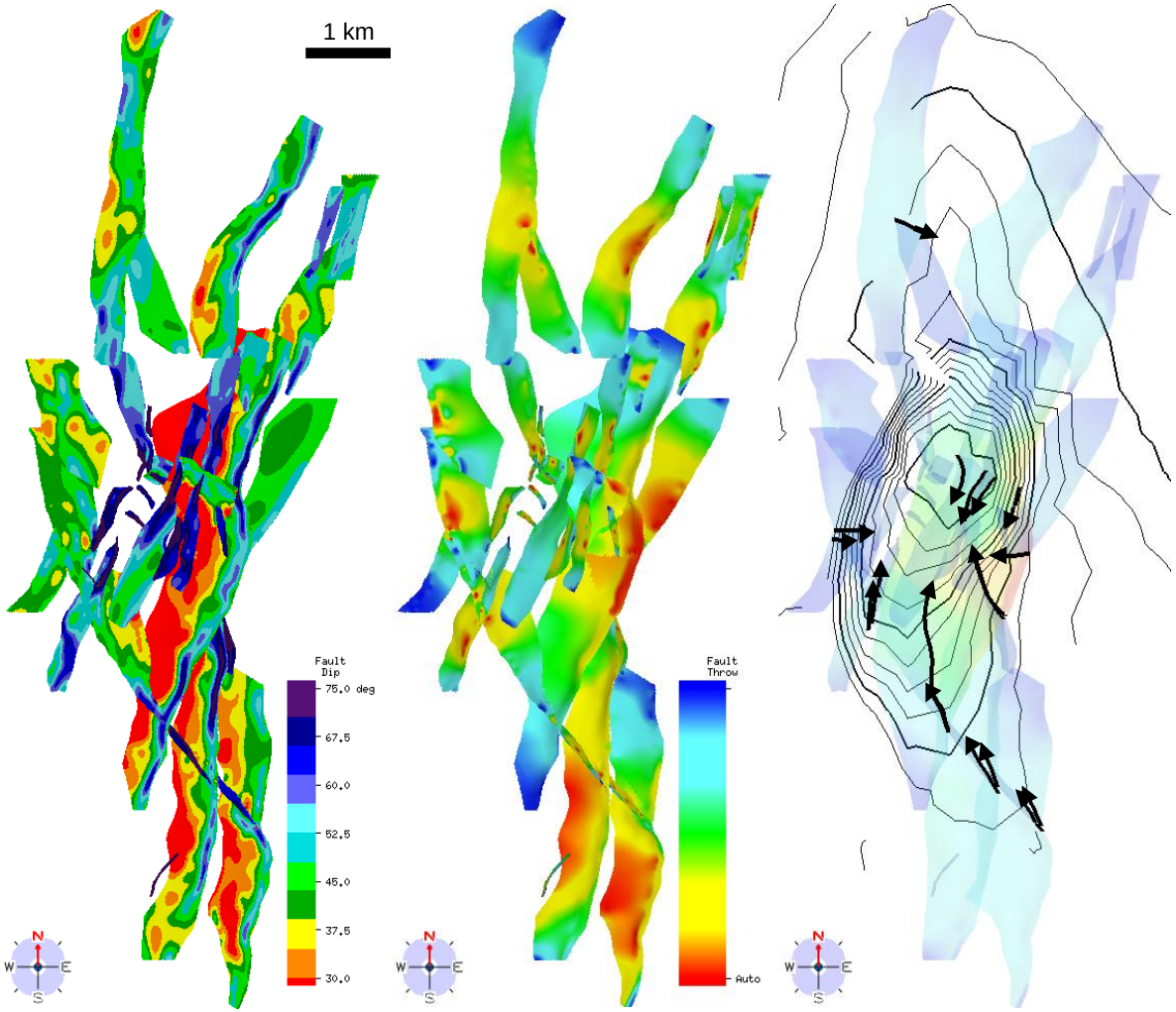

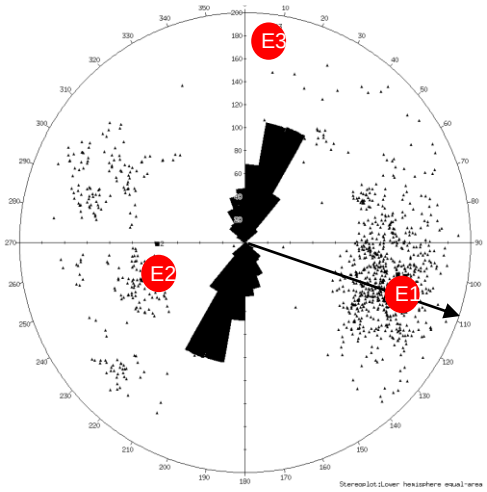

Dip (left), displacement (centre) and branch line orientation (right) of faults.

Stereographic projection and rose diagram (above) of faults showing positions of the cluster and anticluster (E1 and E3)

Regional strain across the structure

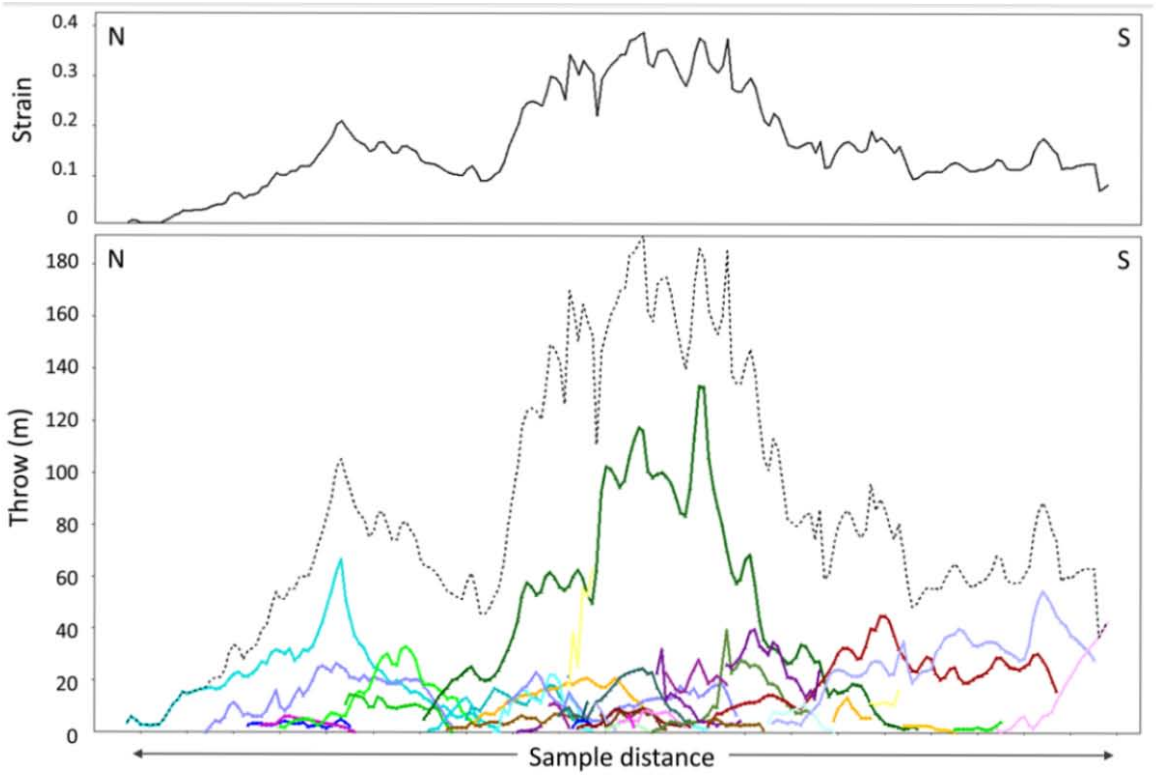

Fig. 5. The lower figure shows the heave profiles of all the framework faults (each individual fault has a unique colour, e.g. Fault F1 is the large green profile in the centre) measured at an azimuth 100°. The summed heaves are represented by the black dotted line. In the upper figure the summed heave is scaled to regional extensional strain (0.4 = 4% extension).

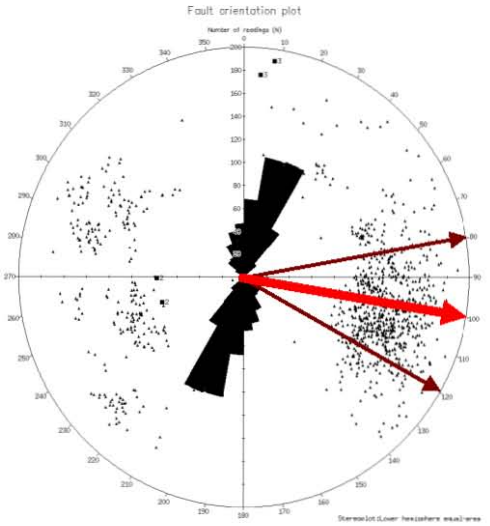

ε_v	ε_{hmin}	ε_{hmax}
0.00	0.00	0.00
−0.03	0.00	0.03
−0.06	0.00	0.06

Large shear fractures in wells

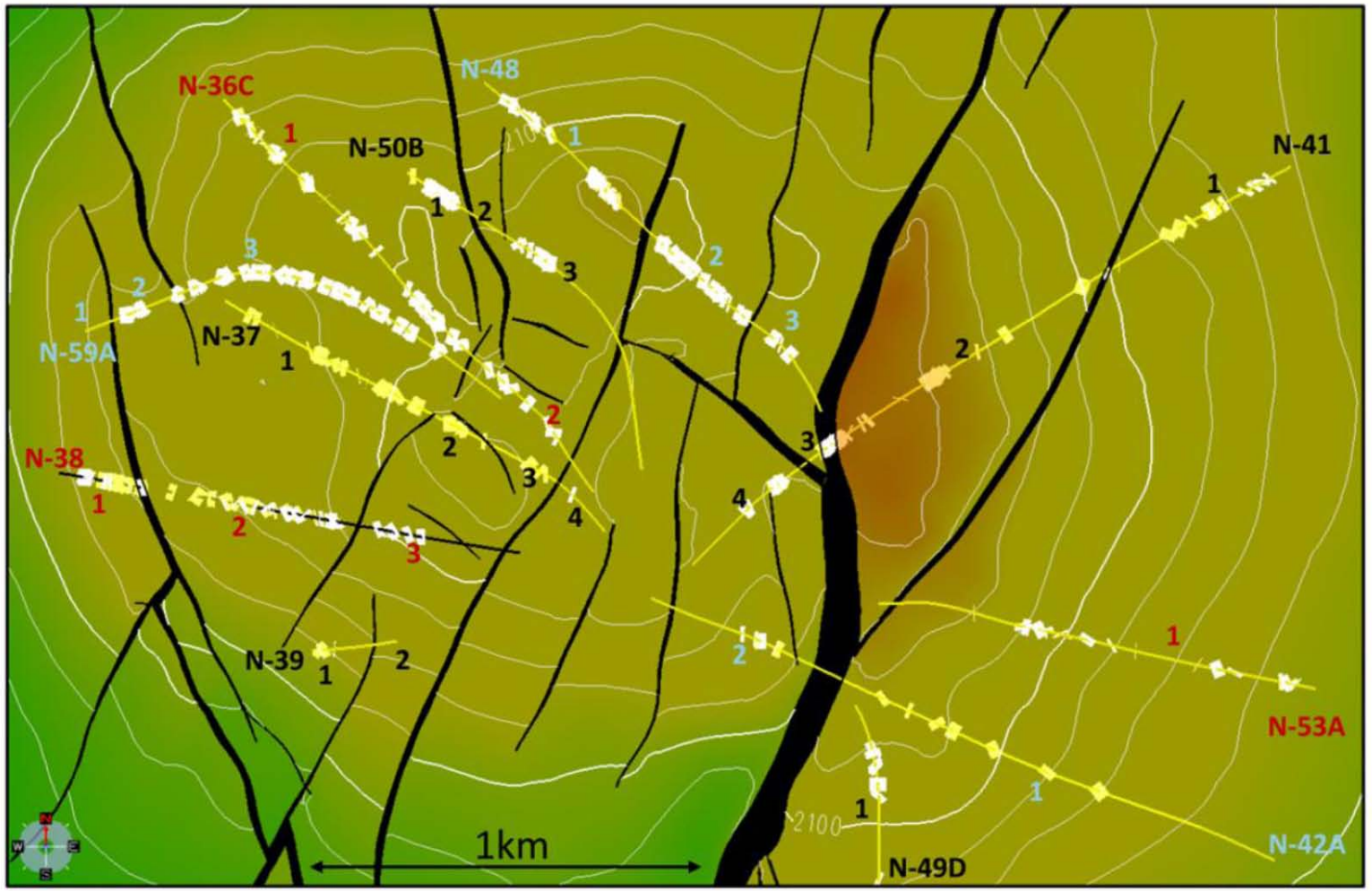

Fig. 3. Structure map of the Top M2 horizon showing wells and major fractures as interpreted from image logs. Labels indicate the structural domains that have been used to compartmentalize the fracture densities.

ED Modelling: Illustration of effects of faults

Fault separations

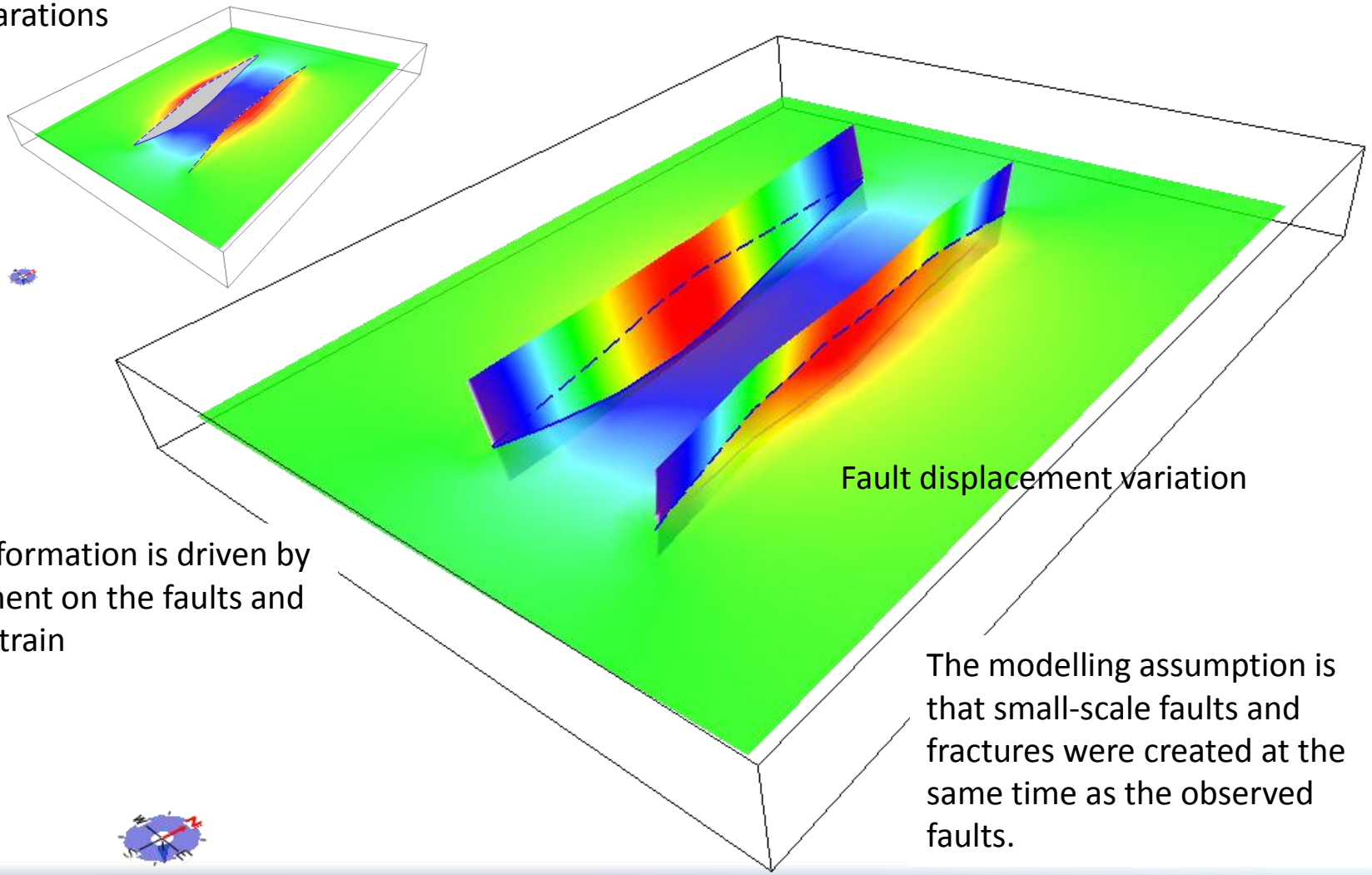

Fault displacement variation

Elastic deformation is driven by displacement on the faults and regional strain

The modelling assumption is that small-scale faults and fractures were created at the same time as the observed faults.

Predicted fracture types

Elastic deformation is driven by displacement on the faults and regional strain

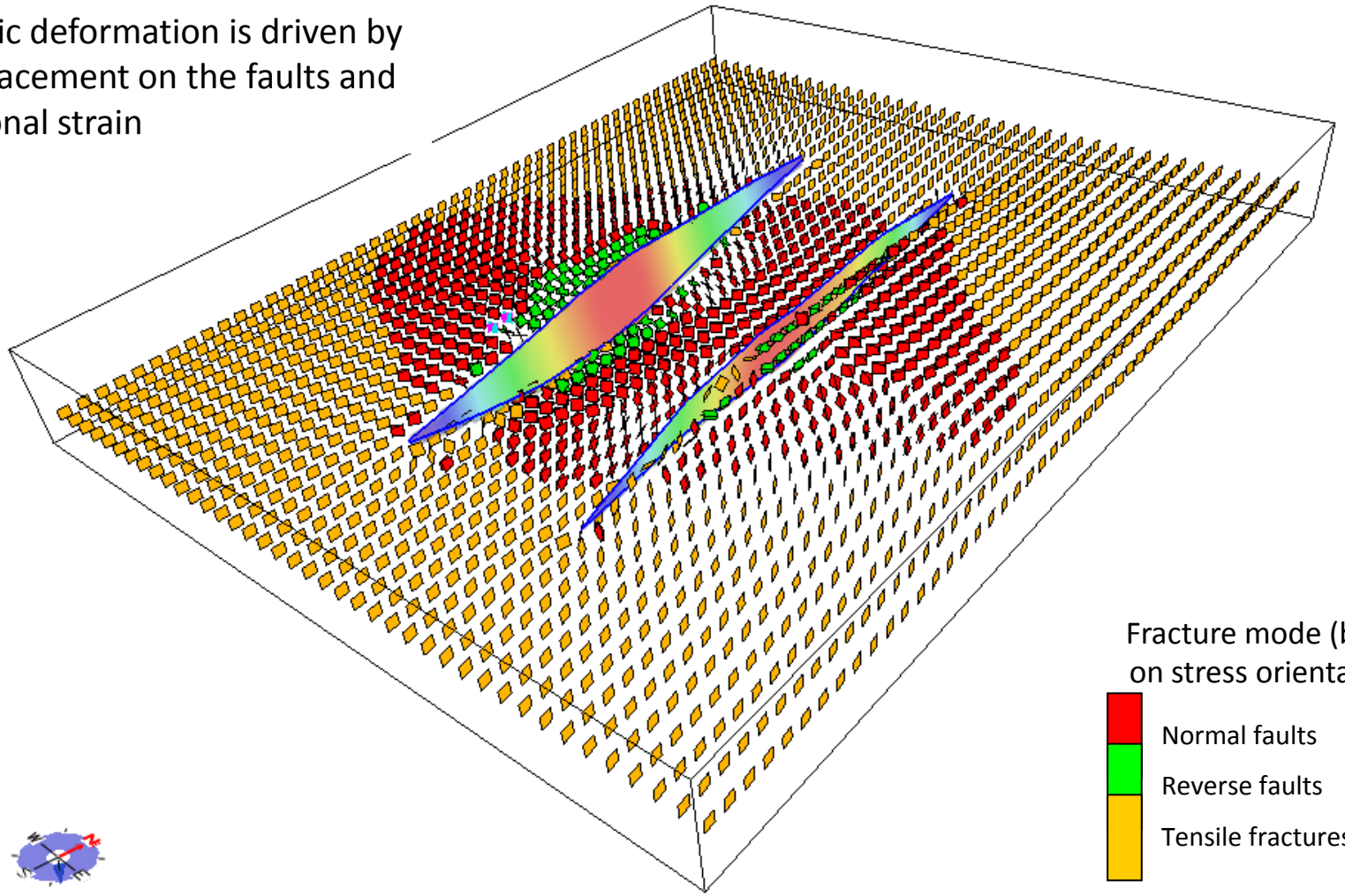

Fracture mode (based on stress orientation)

- Normal faults
- Reverse faults
- Tensile fractures

Predicted fracture intensity

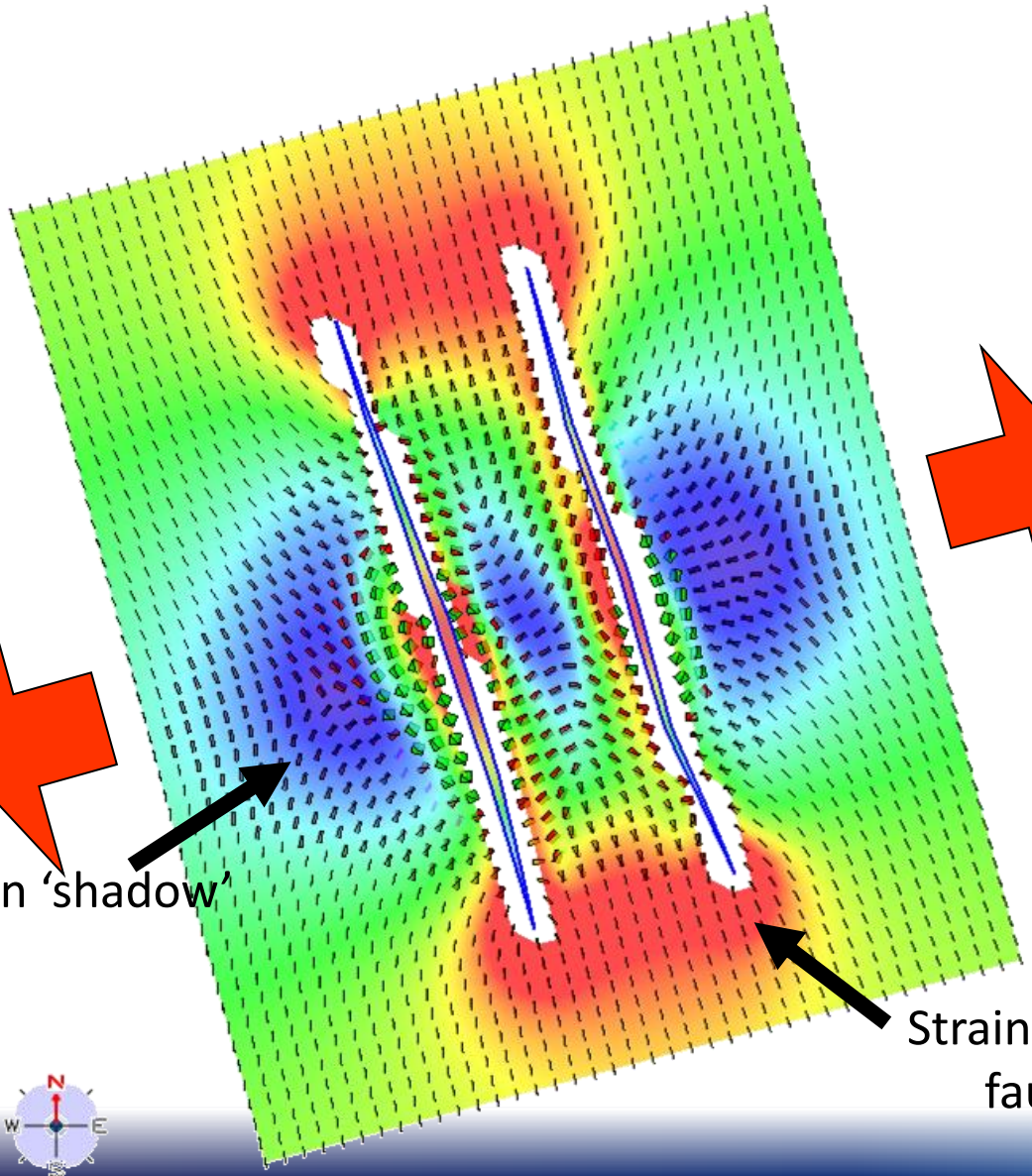

strain ‘shadow’

Strain magnitude concentration at fault tips – more fractures?

It’s assumed that fracture intensity will scale in some way with strain intensity.

There are many ways to represent this but here we use strain magnitude

$$\varepsilon_m = \sqrt{\varepsilon_1^2 + \varepsilon_2^2 + \varepsilon_3^2}$$

Application to the Gorm structure

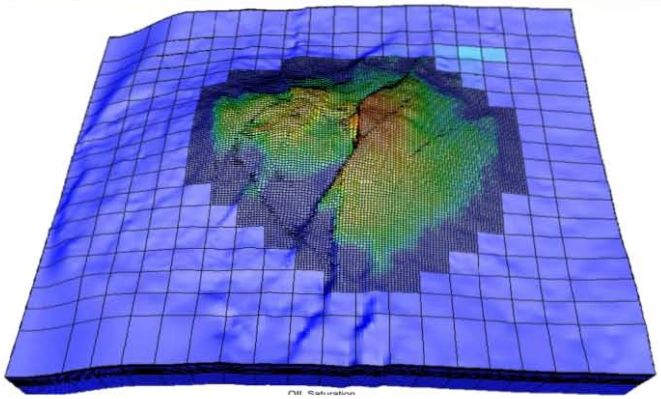

Application to the Gorm structure

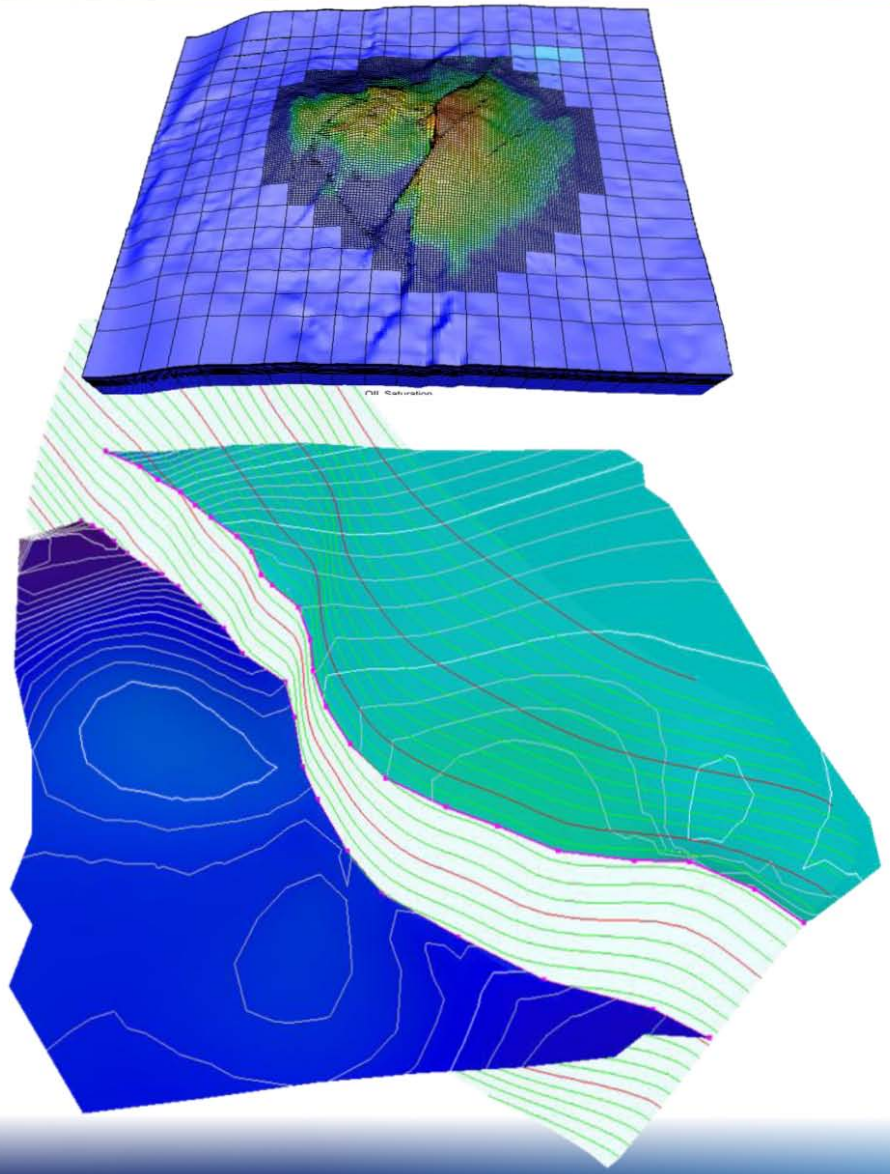

Application to the Gorm structure

Salt intrusion is modelled with triangular, dilation, dislocations with uplift and subsidence relative to a pre-mobile top salt layer

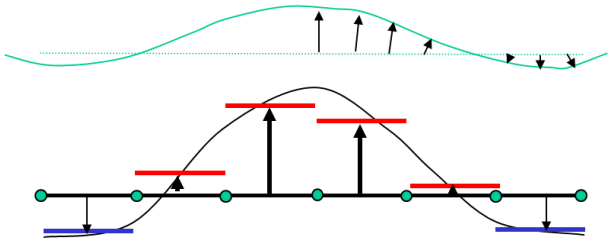

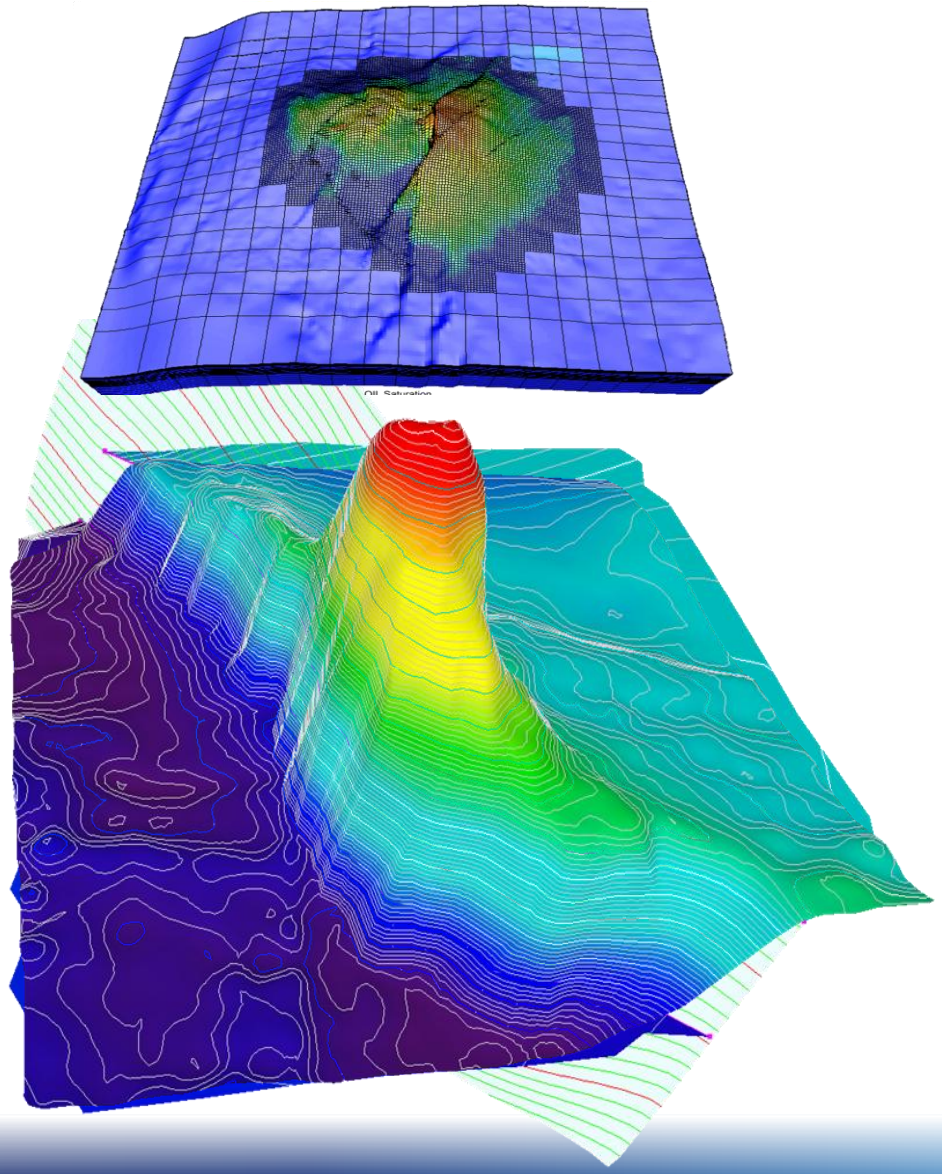

Application to the Gorm structure

Salt intrusion is modelled with triangular, dilation, dislocations with uplift and subsidence relative to a pre-mobile top salt layer

The faults in the reservoir are modelled as sets of shear dislocations in a broadly E-W extensional regime

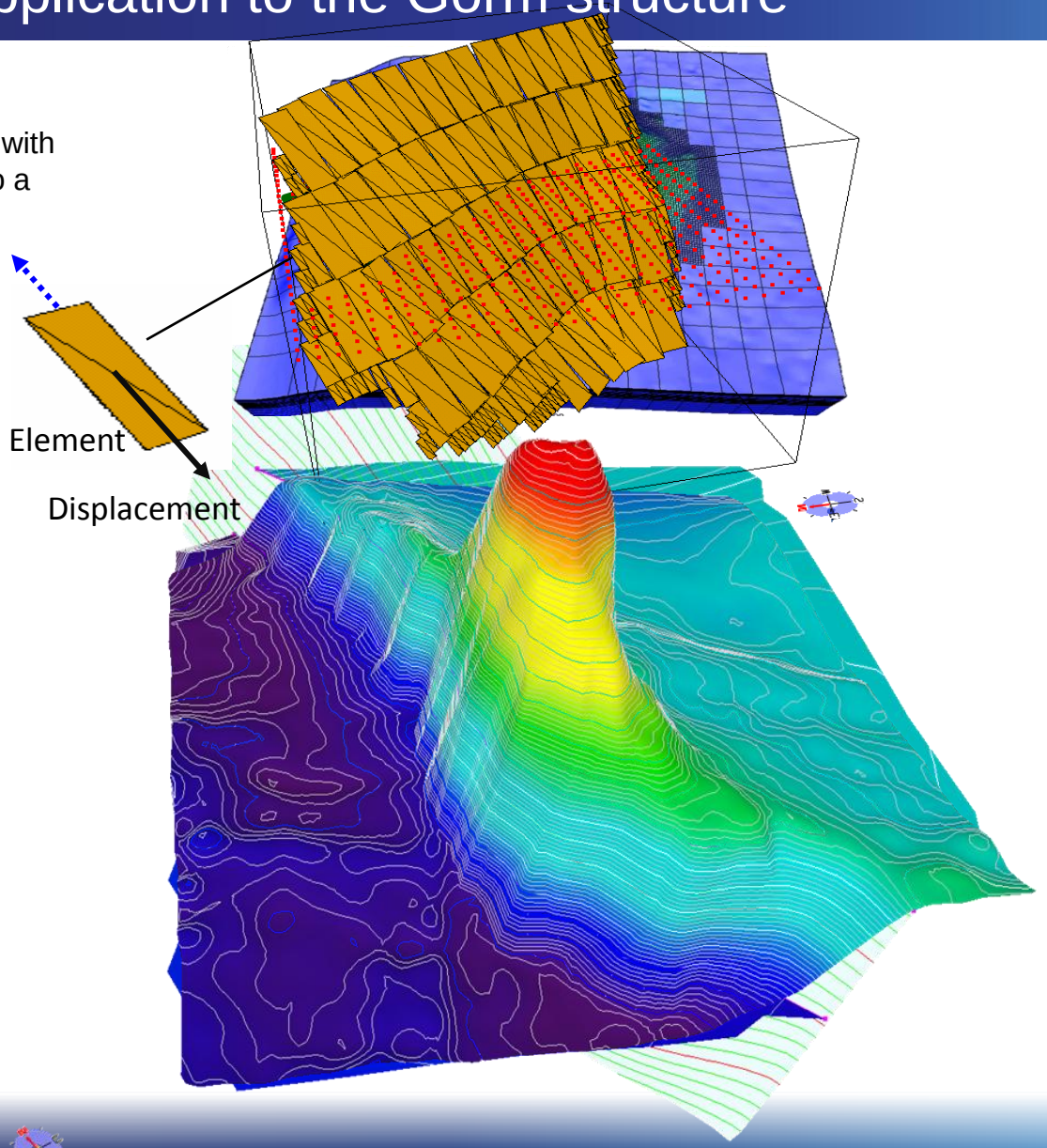

Application to the Gorm structure

Salt intrusion is modelled with triangular, dilation, dislocations with uplift and subsidence relative to a pre-mobile top salt layer

The faults in the reservoir are modelled as sets of shear dislocations in a broadly E-W extensional regime

At each observation point the total strains are calculated which lead to the orientations and magnitudes of the principal stress, the orientation and mode of failure for sub-seimic fractures

An observation point can be on an horizon surface, a grid or importantly at the location of an observed fracture in a well

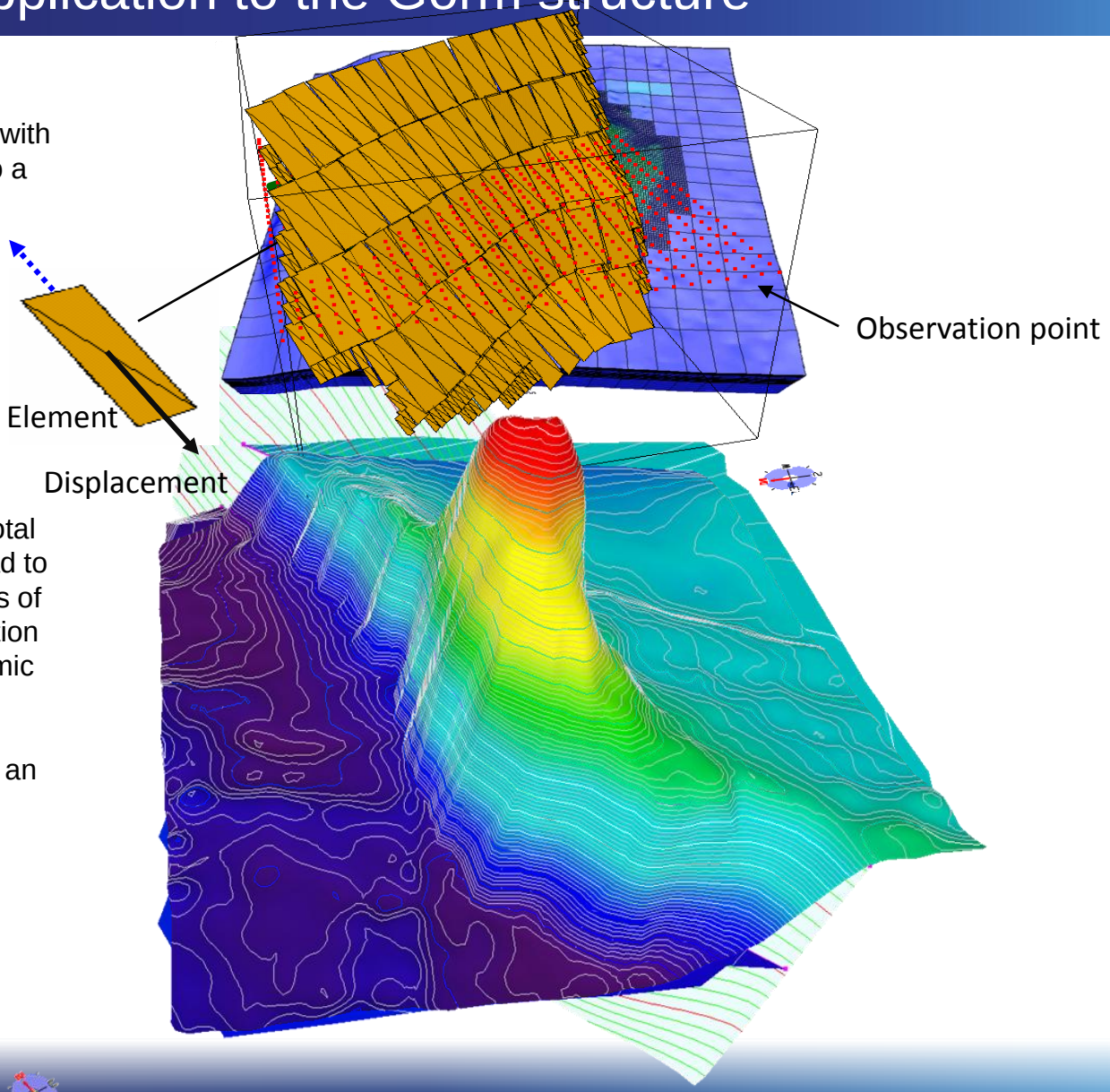

Application to the Gorm structure

Salt intrusion is modelled with triangular, dilation, dislocations with uplift and subsidence relative to a pre-mobile top salt layer

The faults in the reservoir are modelled as sets of shear dislocations in a broadly E-W extensional regime

At each observation point the total strains are calculated which lead to the orientations and magnitudes of the principal stress, the orientation and mode of failure for sub-seimic fractures

An observation point can be on an horizon surface, a grid or importantly at the location of an observed fracture in a well

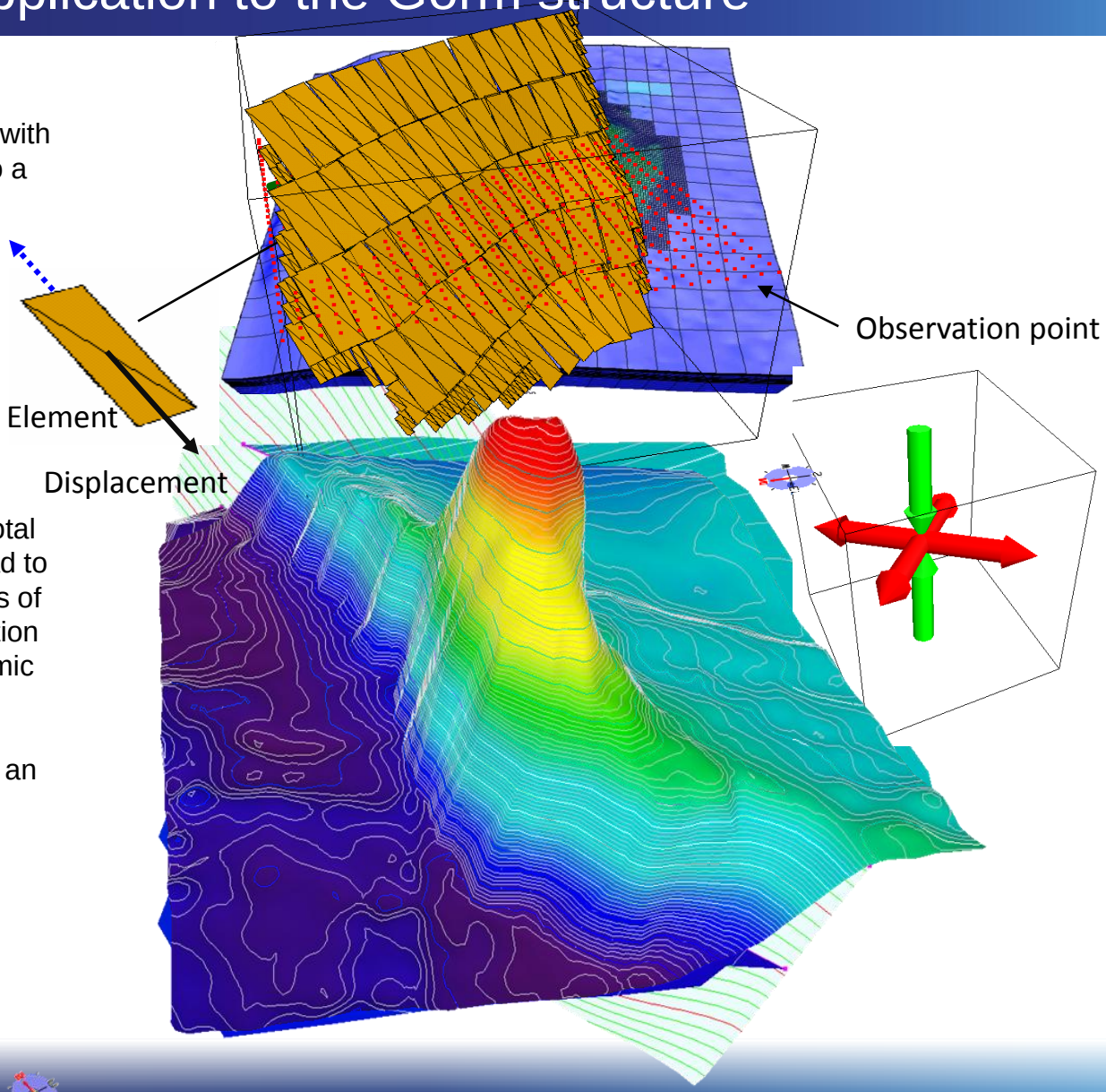

Application to the Gorm structure

Salt intrusion is modelled with triangular, dilation, dislocations with uplift and subsidence relative to a pre-mobile top salt layer

The faults in the reservoir are modelled as sets of shear dislocations in a broadly E-W extensional regime

At each observation point the total strains are calculated which lead to the orientations and magnitudes of the principal stress, the orientation and mode of failure for sub-seimic fractures

An observation point can be on an horizon surface, a grid or importantly at the location of an observed fracture in a well

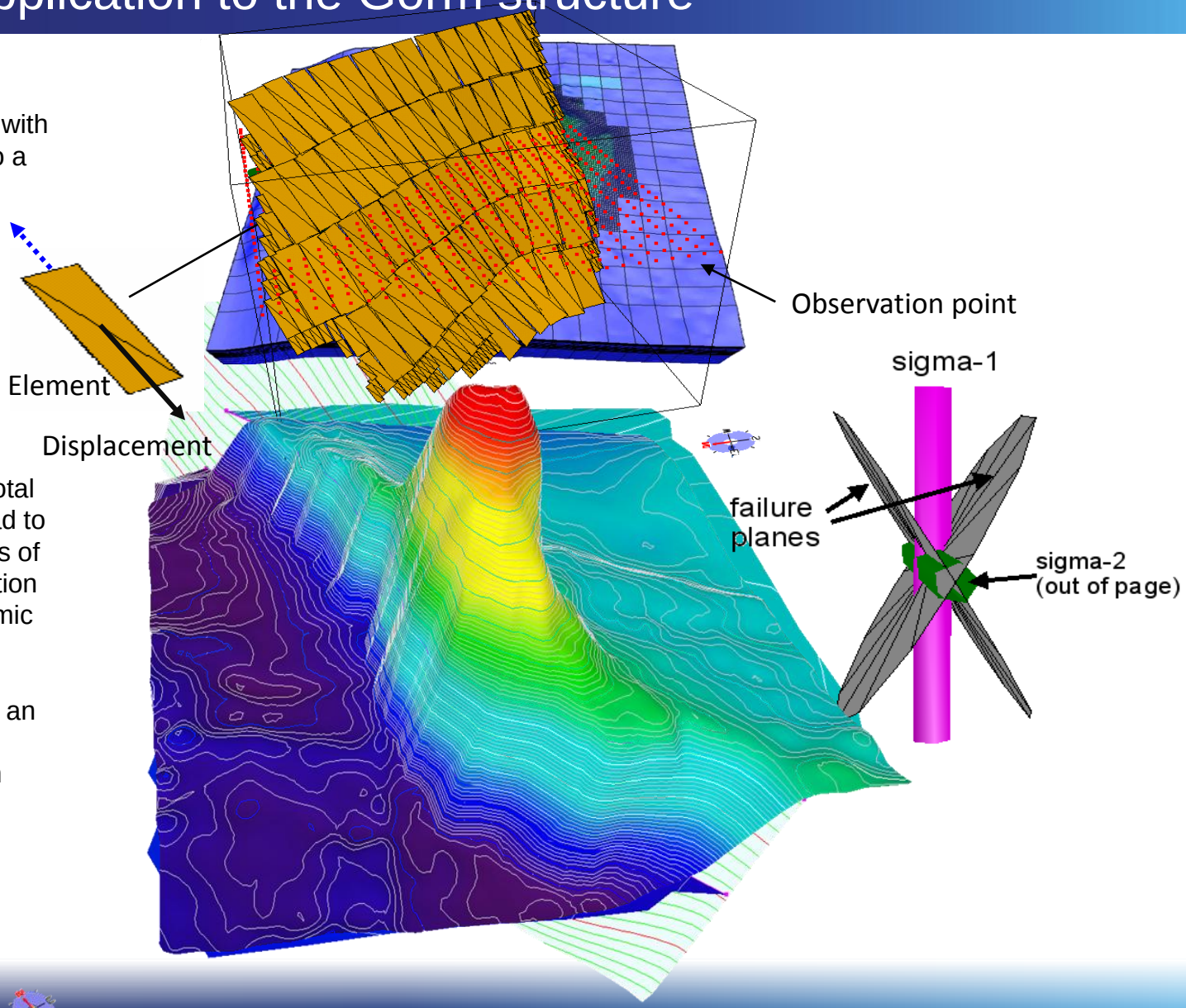

Application to the Gorm structure

Salt intrusion is modelled with triangular, dilation, dislocations with uplift and subsidence relative to a pre-mobile top salt layer

The faults in the reservoir are modelled as sets of shear dislocations in a broadly E-W extensional regime

At each observation point the total strains are calculated which lead to the orientations and magnitudes of the principal stress, the orientation and mode of failure for sub-seimic fractures

An observation point can be on an horizon surface, a grid or importantly at the location of an observed fracture in a well

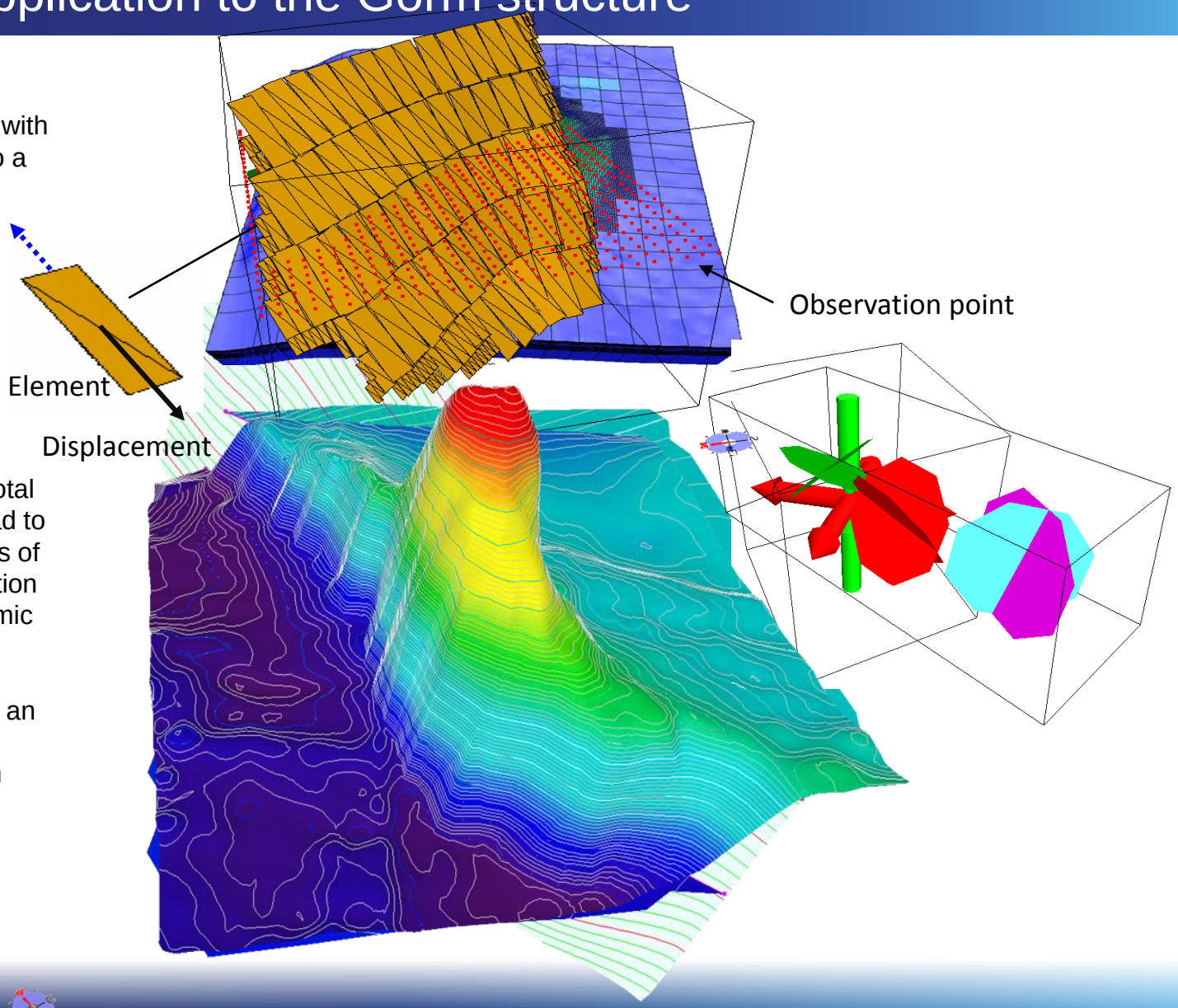

Application to the Gorm structure

Salt intrusion is modelled with triangular, dilation, dislocations with uplift and subsidence relative to a pre-mobile top salt layer

The faults in the reservoir are modelled as sets of shear dislocations in a broadly E-W extensional regime

At each observation point the total strains are calculated which lead to the orientations and magnitudes of the principal stress, the orientation and mode of failure for sub-seimic fractures

An observation point can be on an horizon surface, a grid or importantly at the location of an observed fracture in a well

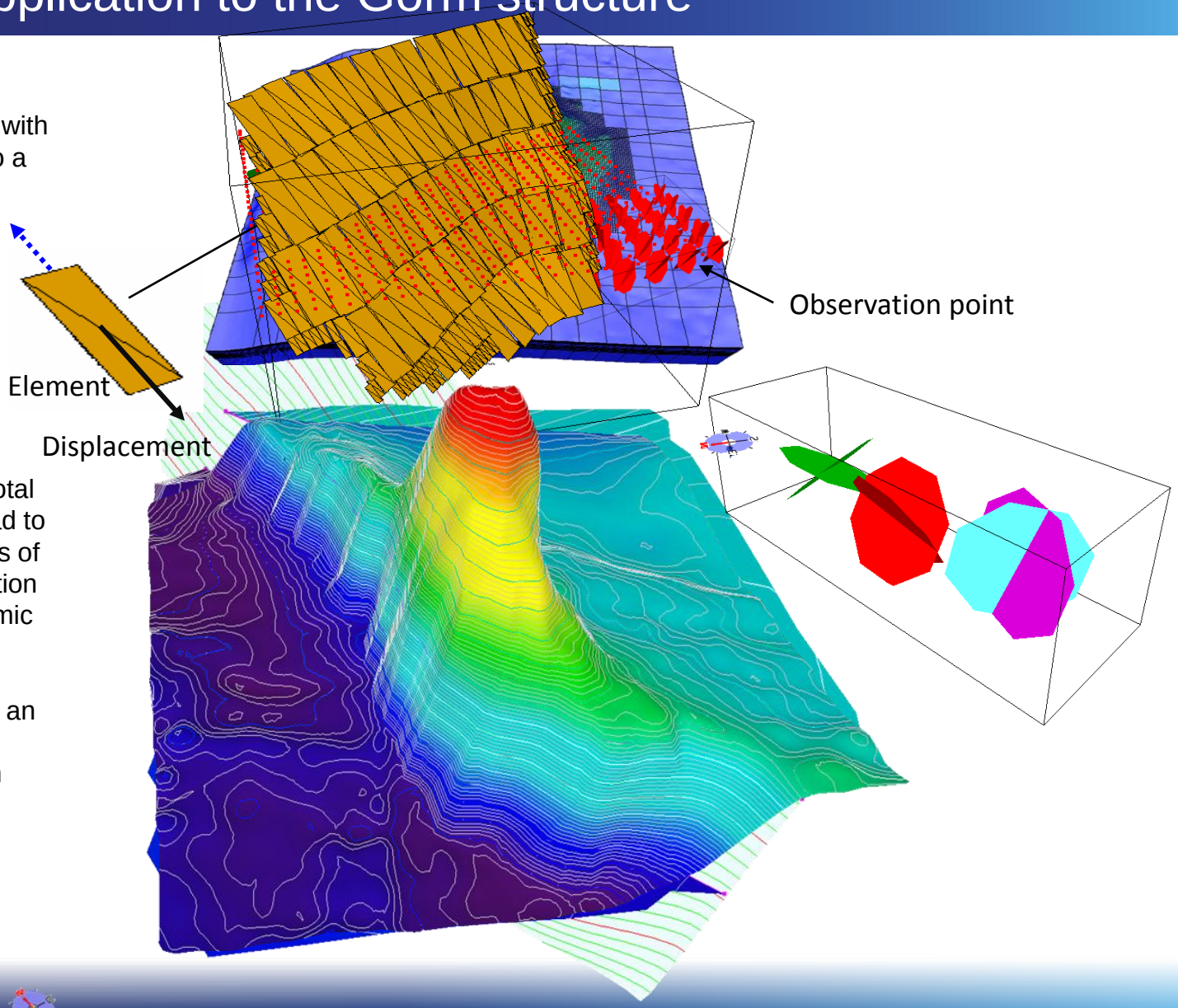

Model cofigurations

Table 1. *Summary table of mnemonics of mechanical boundary configurations*

	Allochthonous salt (uplift only)			Autochthonous salt		
Scale factor for influence of salt	0	0.5	1	0	0.5	1
Exclude faults	–	SAF0S0	SBF0S0	–	SAF0S1	SBF0S1
Include faults	S0F1	SAF1S0	SBF1S0	–	SAF1S1	SBF1S1

The prefixes S0, SA and SB refer to the influence of the salt used in a run: S0 = none; SA = half; SB = full influence. The middle acronyms refer to the influence of the fault: F0 for no influence and F1 for full. The suffixes S0 and S1 refer to no subsidence and subsidence, respectively.

Table 2. *Three sets of values of remote boundary strains used during the tests on each model-run*

ε_v	ε_{hmin}	ε_{hmax}
0.00	0.00	0.00
−0.03	0.00	0.03
−0.06	0.00	0.06

We also investigated the sensitivity of these models to

(a) variation in orientation of tectonic extension

(b) Variation in coefficient of internal friction between 0.2 and 1.0 (0.55 being preferred)

Model cofigurations

Table 1. *Summary table of mnemonics of mechanical boundary configurations*

	Allochthonous salt (uplift only)			Autochthonous salt		
Scale factor for influence of salt	0	0.5	1	0	0.5	1
Exclude faults				–	SAF0S1	SBF0S1
Include faults				–	SAF1S1	SBF1S1

The prefixes S0, SA and SB r
nyms refer to the influence
subsidence, respectively.

half; SB = full influence. The middle acro-
es S0 and S1 refer to no subsidence and

Continuous in-flow of salt: no withdrawal or subsidence

Table 2. *Three sets of values of remote boundary strains used during the tests on each model-run*

ε_v	ε_{hmin}	ε_{hmax}
0.00	0.00	0.00
−0.03	0.00	0.03
−0.06	0.00	0.06

We also investigated the sensitivity of these models to

(a) variation in orientation of tectonic extension

(b) Variation in coefficient of internal friction between 0.2 and 1.0 (0.55 being preferred)

Model cofigurations

Table 1. *Summary table of mnemonics of mechanical boundary configurations*

	Allochthonous salt (uplift only)			Autochthonous salt		
Scale factor for influence of salt	0	0.5	1	0	0.5	1
Exclude faults	–	SAF0S0	SBF0S0			
Include faults	S0F1	SAF1S0	SBF1S			

The prefixes S0, SA and SB refer to the influence of the salt used in a run: S0 = nyms refer to the influence of the fault: F0 for no influence and F1 for ful subsidence, respectively.

Local salt: uplift and subsidence

Table 2. *Three sets of values of remote boundary strains used during the tests on each model-run*

ε_v	ε_{hmin}	ε_{hmax}
0.00	0.00	0.00
−0.03	0.00	0.03
−0.06	0.00	0.06

We also investigated the sensitivity of these models to

(a) variation in orientation of tectonic extension

(b) Variation in coefficient of internal friction between 0.2 and 1.0 (0.55 being preferred)

Model cofigurations

Table 1. *Summary table of mnemonics of mechanical boundary configurations*

	Allochthonous salt (uplift only)			Autochthonous salt		
Scale factor for influence of salt	0	0.5	1	0	0.5	1
Exclude faults	–	SAF0S0	SBF0S0	–	SAF0S1	SBF0S1
Include faults	S0F1	SAF1S0	SBF1S0	–	SAF1S1	SBF1S1

The prefixes S0, SA and SB refer to the influence of the salt used in a run: S0 = none; SA = half; SB = full influence. The middle acronyms refer to the influence of the fault: F0 for no influence and F1 for full. The suffixes S0 and S1 refer to no subsidence and subsidence, respectively.

Table 2. *Three sets of values of remote boundary strains used during the tests on each model-run*

ε_v	ε_{hmin}	ε_{hmax}
0.00	0.00	0.00
−0.03	0.00	0.03
−0.06	0.00	0.06

We also investigated the sensitivity of these models to

(a) variation in orientation of tectonic extension

(b) Variation in coefficient of internal friction between 0.2 and 1.0 (0.55 being preferred)

Model cofigurations

Table 1. *Summary table of mnemonics of mechanical boundary configurations*

	Allochthonous salt (uplift only)			Autochthonous salt		
Scale factor for influence of salt	0	0.5	1	0	0.5	1
Exclude faults				SAF0S1		SBF0S1
Include faults				SAF1S1		SBF1S1

The prefixes S0, SA and SB refer nyms refer to the influence of t subsidence, respectively.

= full influence. The middle acro- ıd S1 refer to no subsidence and

Vary the impact of salt: No effect, half effect, full effect

Table 2. *Three sets of values of remote boundary strains used during the tests on each model-run*

ε_v	ε_{hmin}	ε_{hmax}
0.00	0.00	0.00
−0.03	0.00	0.03
−0.06	0.00	0.06

We also investigated the sensitivity of these models to

(a) variation in orientation of tectonic extension

(b) Variation in coefficient of internal friction between 0.2 and 1.0 (0.55 being preferred)

Gorm field: restored Top M2 without/with salt

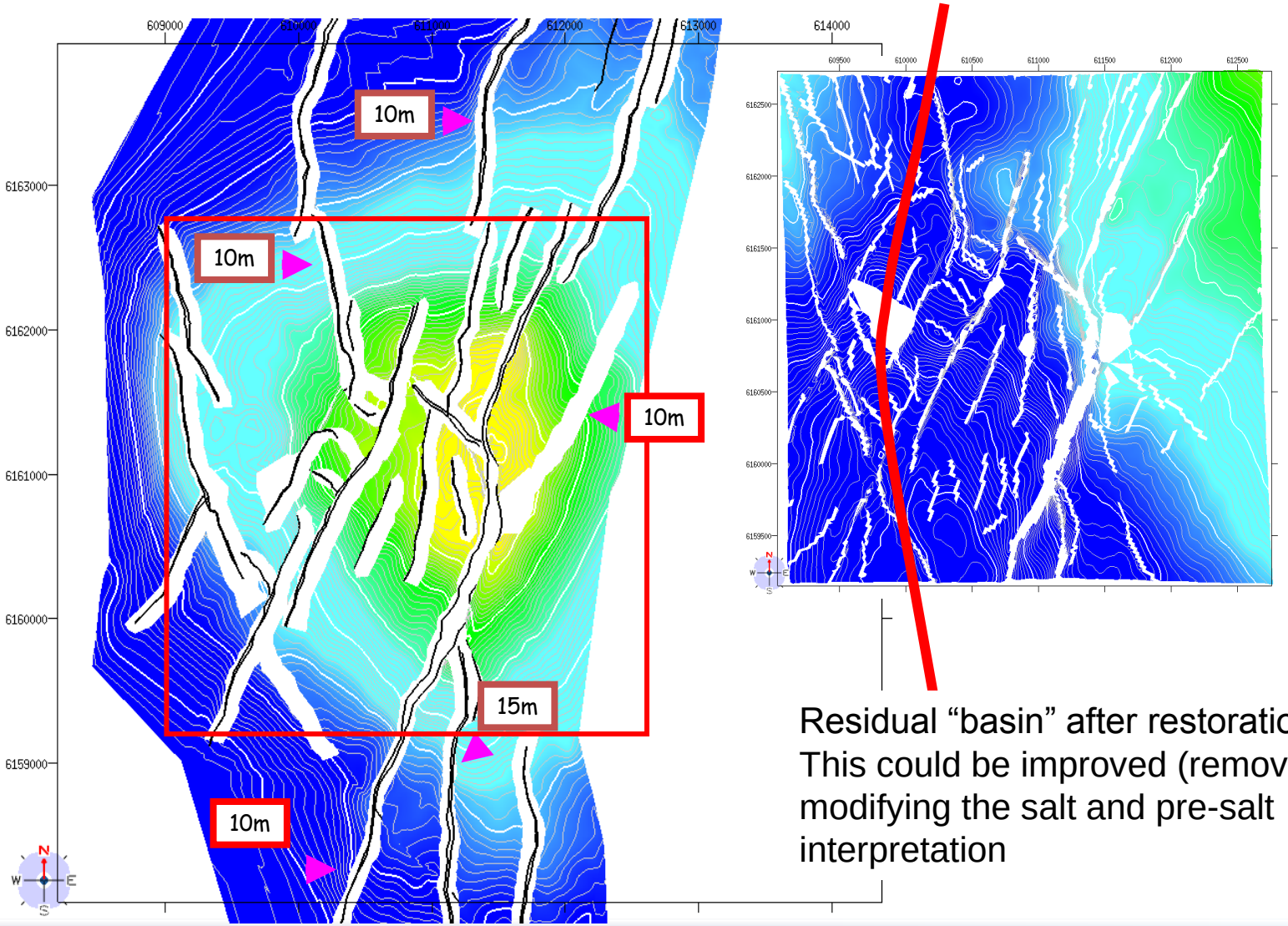

Residual “basin” after restoration. This could be improved (removed) by modifying the salt and pre-salt interpretation

Orientation comparison and analysis

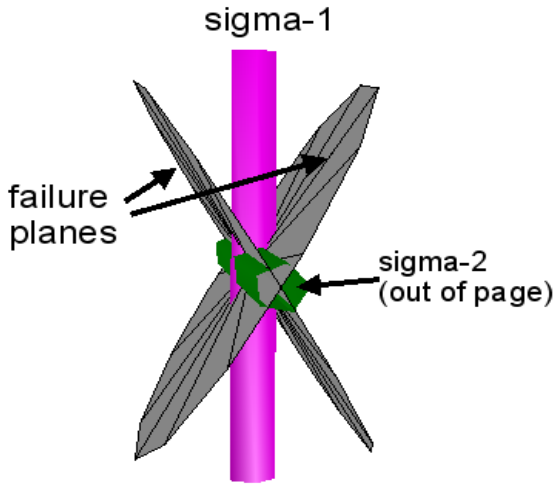

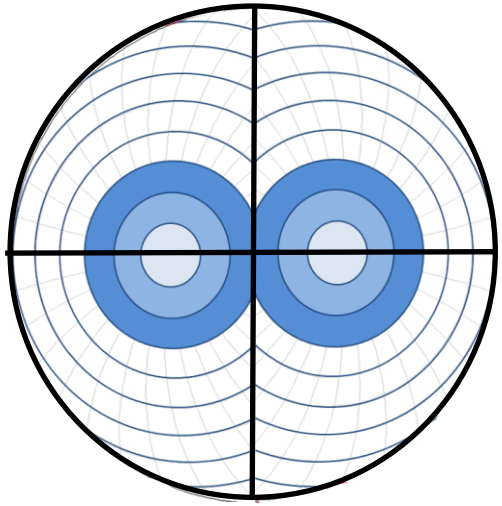

We observe a single fracture

We MODEL a conjugate pair at the same location (our models created very few tensile fractures)

We MEASURE the smallest difference in angle between the poles of the modelled and observed fractures (Δp)

Our null hypothesis states that the orientations of natural fractures is random

The distribution of Δp for the null hypothesis is not uniform

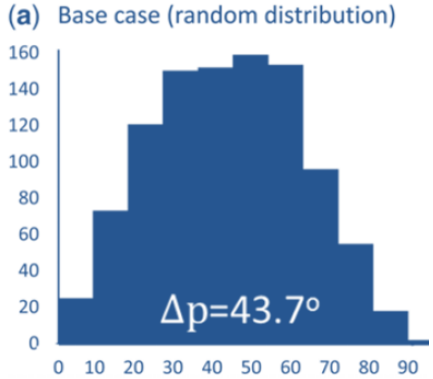

We test the null hypothesis using the Kolmogorov-Smirnov statistic at the 5% level of confidence

Calibration of fracture orientation

All models configurations produce Δp distributions that allow us to reject the null hypothesis at 5% confidence level

However, orientation mismatch is greatest when salt is excluded and least with full-effect of local salt with uplift and subsidence

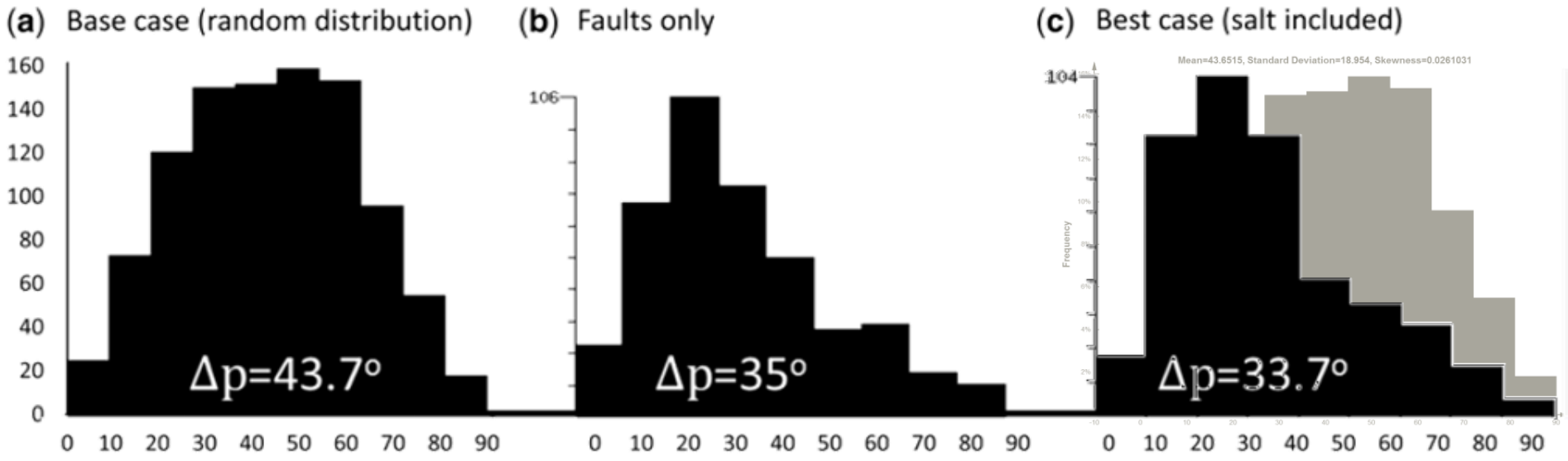

Calibration of fracture orientation

All models configurations produce Δp distributions that allow us to reject the null hypothesis at 5% confidence level

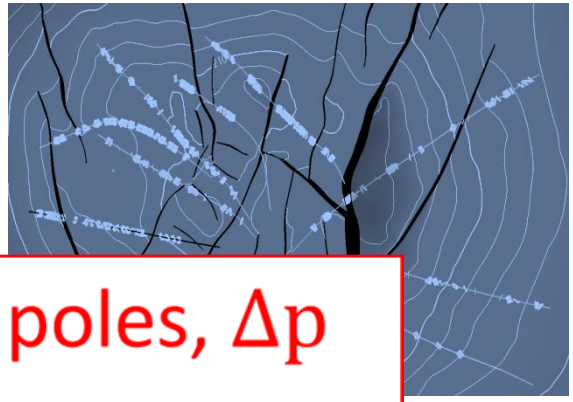

However, salt is exc with uplift

Angular difference between poles, Δp

mean	33.7°
median	29.7°
75th percentile	44.0°

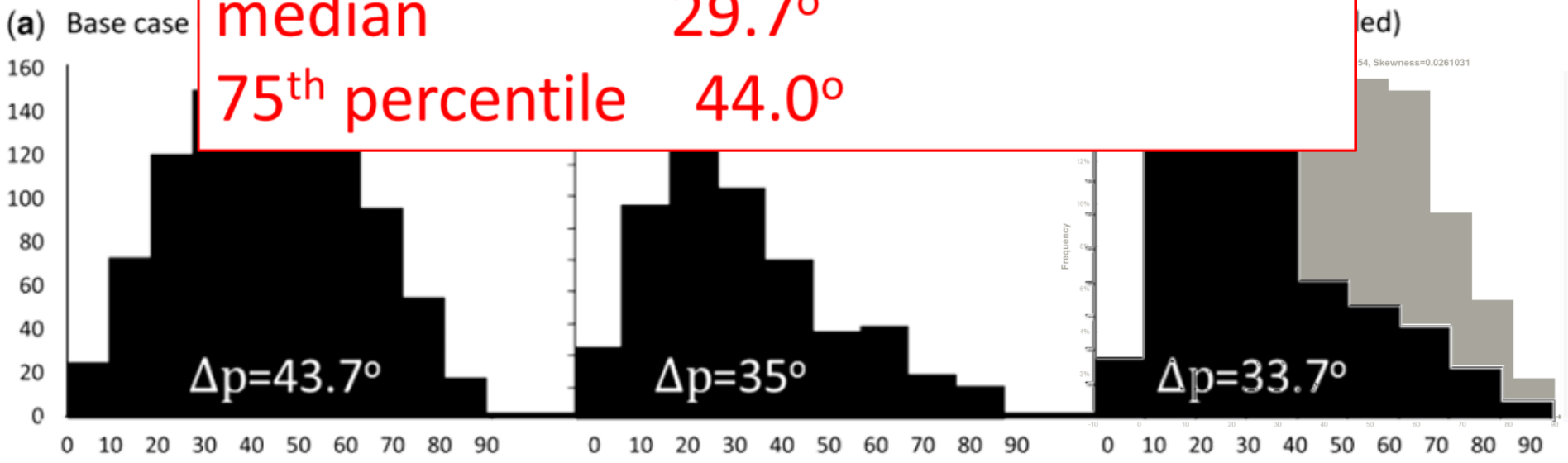

Deformation intensity vs depletion

Densely fractured hot areas, sparsely fractured cold

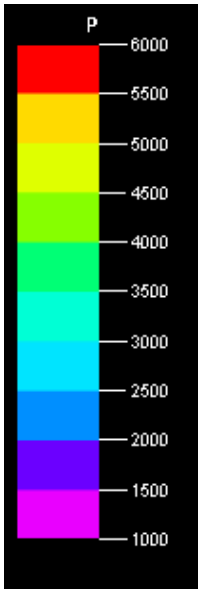

Pore fluid pressure (psi). Virgin pressures between 4000 psi and 4500 psi

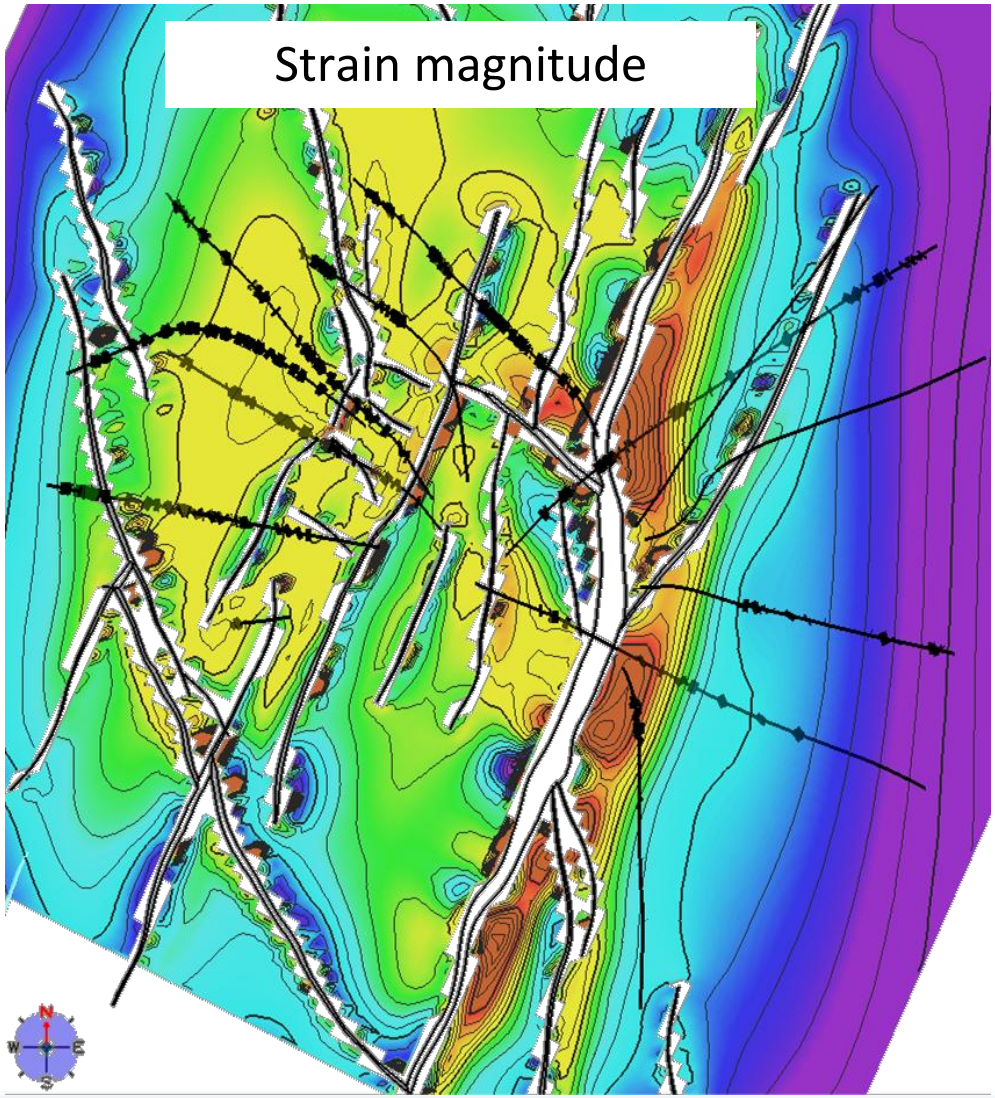

Well tracks with logged major faults/fractures

Flipping between the two image there is a clear and strong correspondence between depletion (blue) and high strain magnitude (red)

Deformation intensity vs depletion

Densely fractured hot areas, sparsely fractured cold

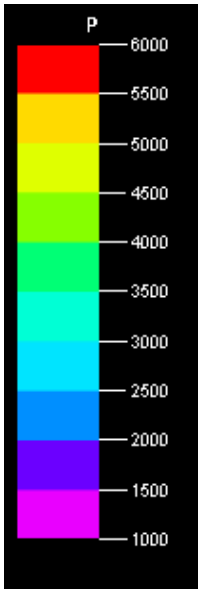

Pore fluid pressure (psi). Virgin pressures between 4000 psi and 4500 psi

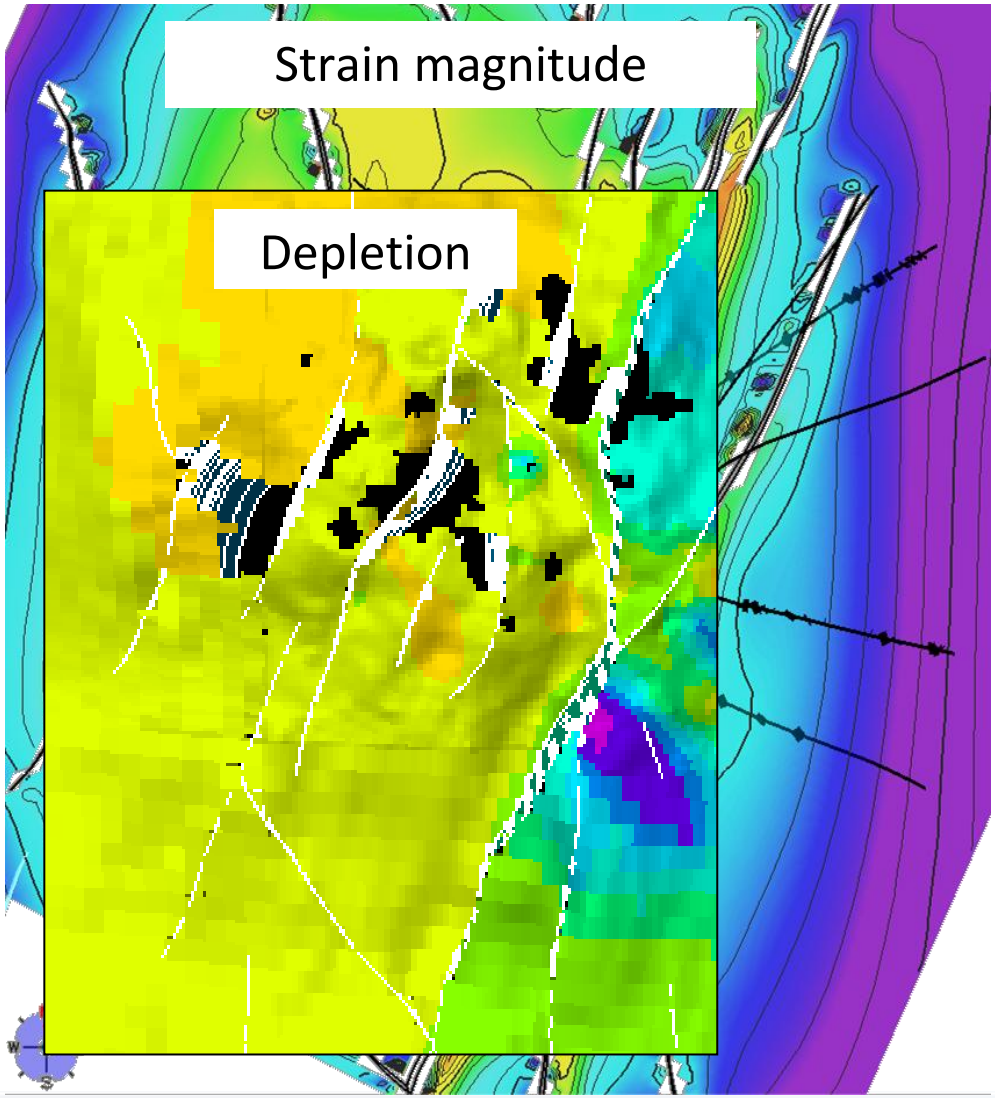

Well tracks with logged major faults/fractures

Flipping between the two image there is a clear and strong correspondence between depletion (blue) and high strain magnitude (red)

Fracture density calibration, local domains

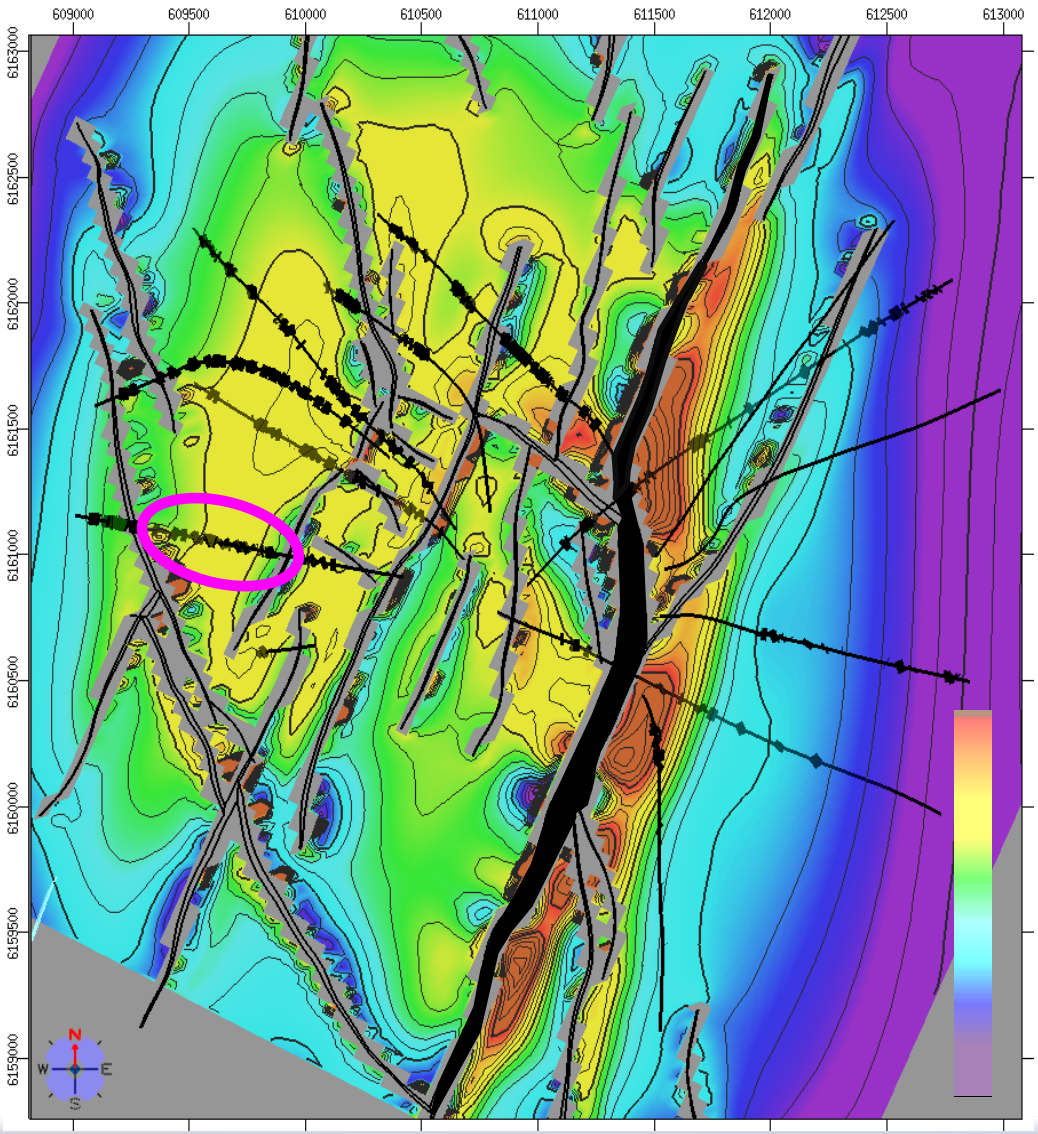

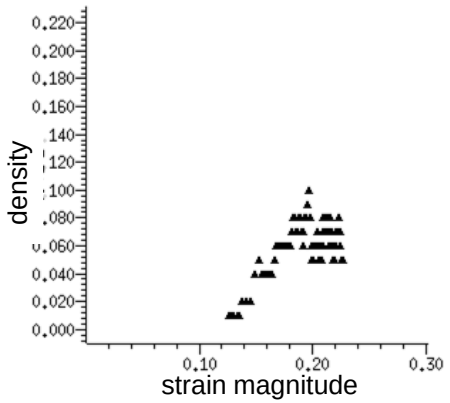

Fracture density calibration, local domains

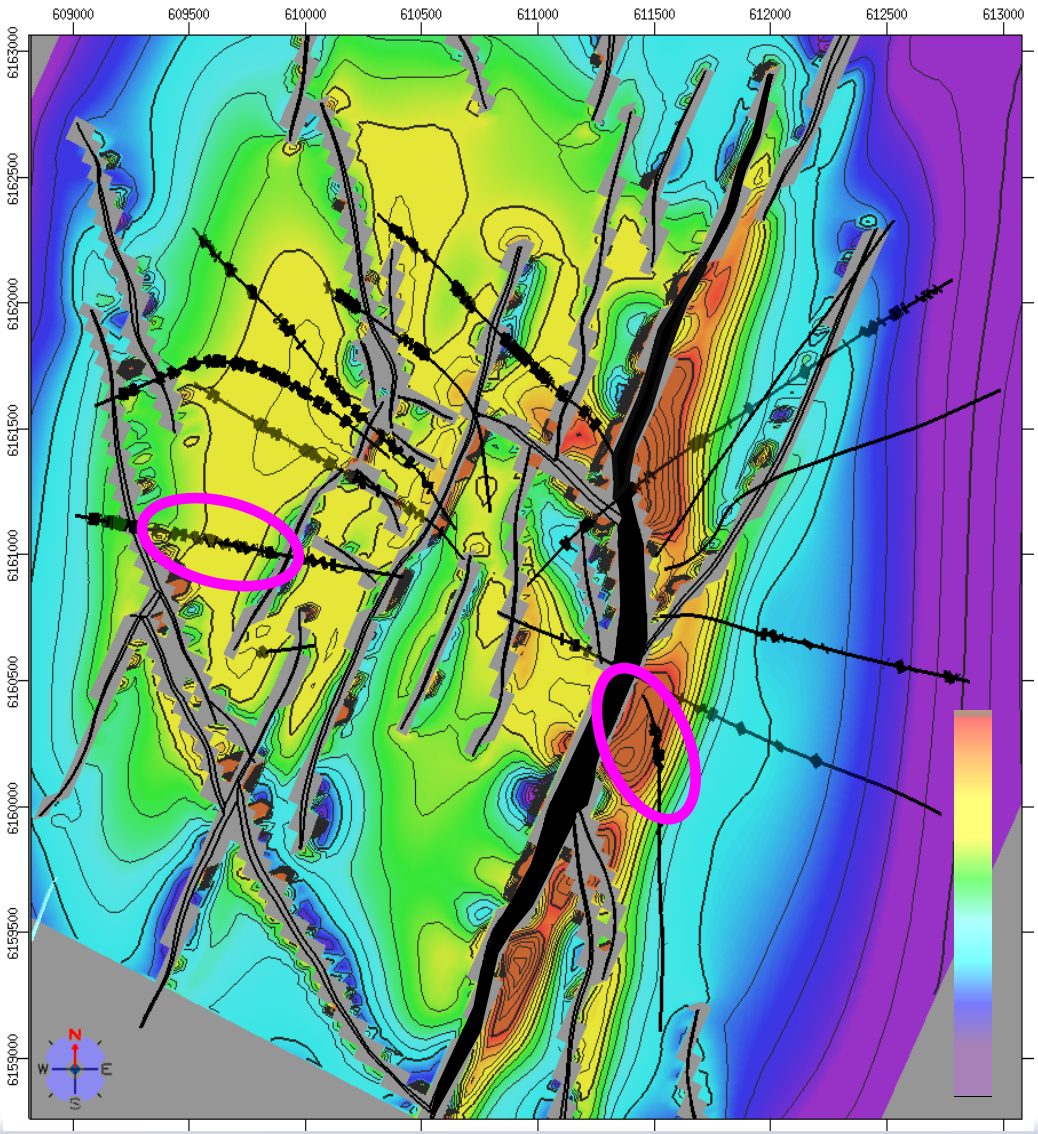

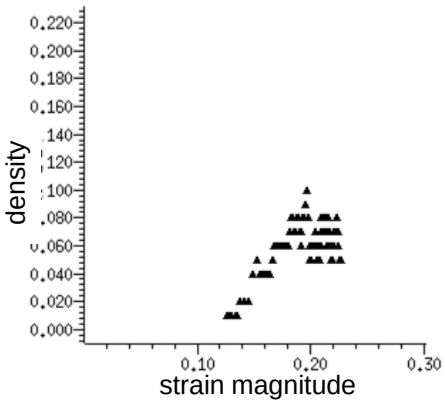

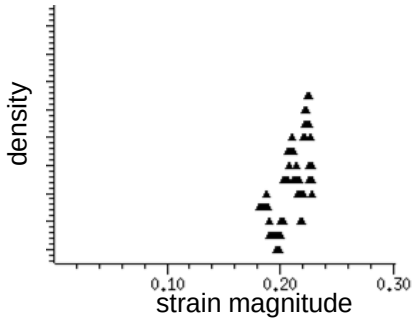

Fracture density calibration, local domains

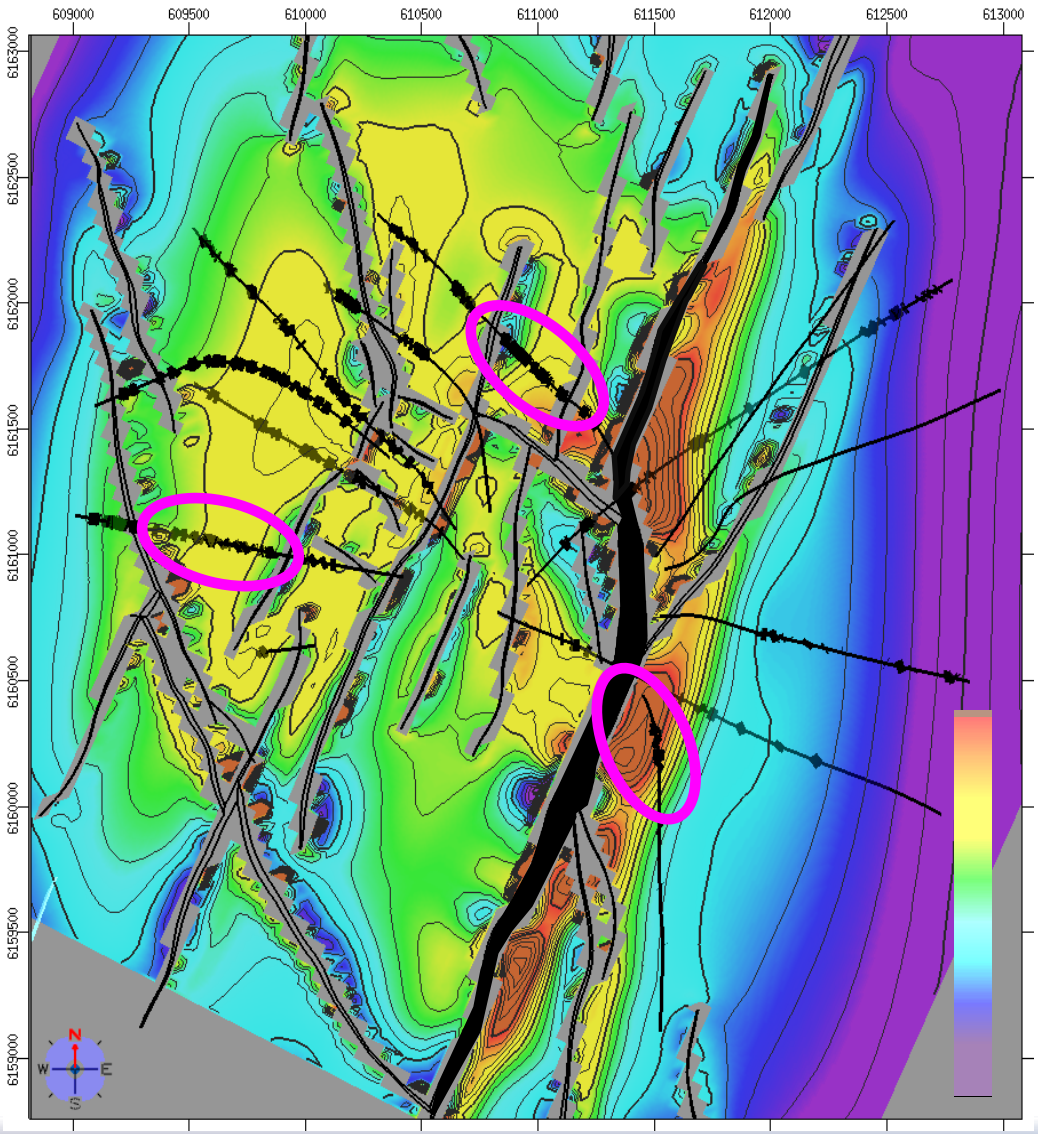

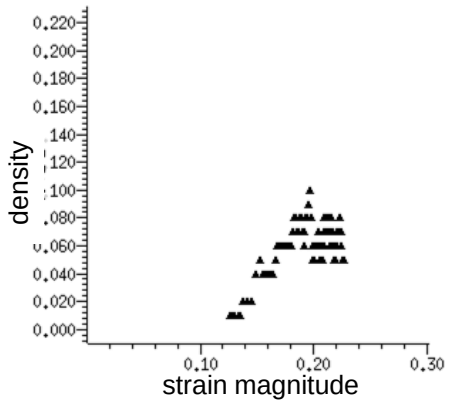

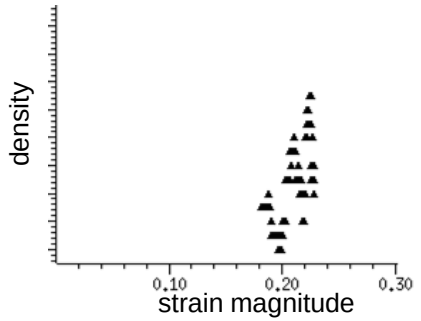

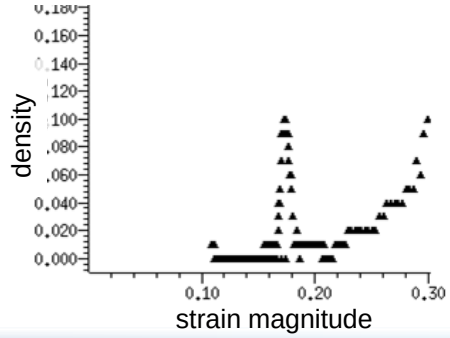

Fracture density calibration, all domains

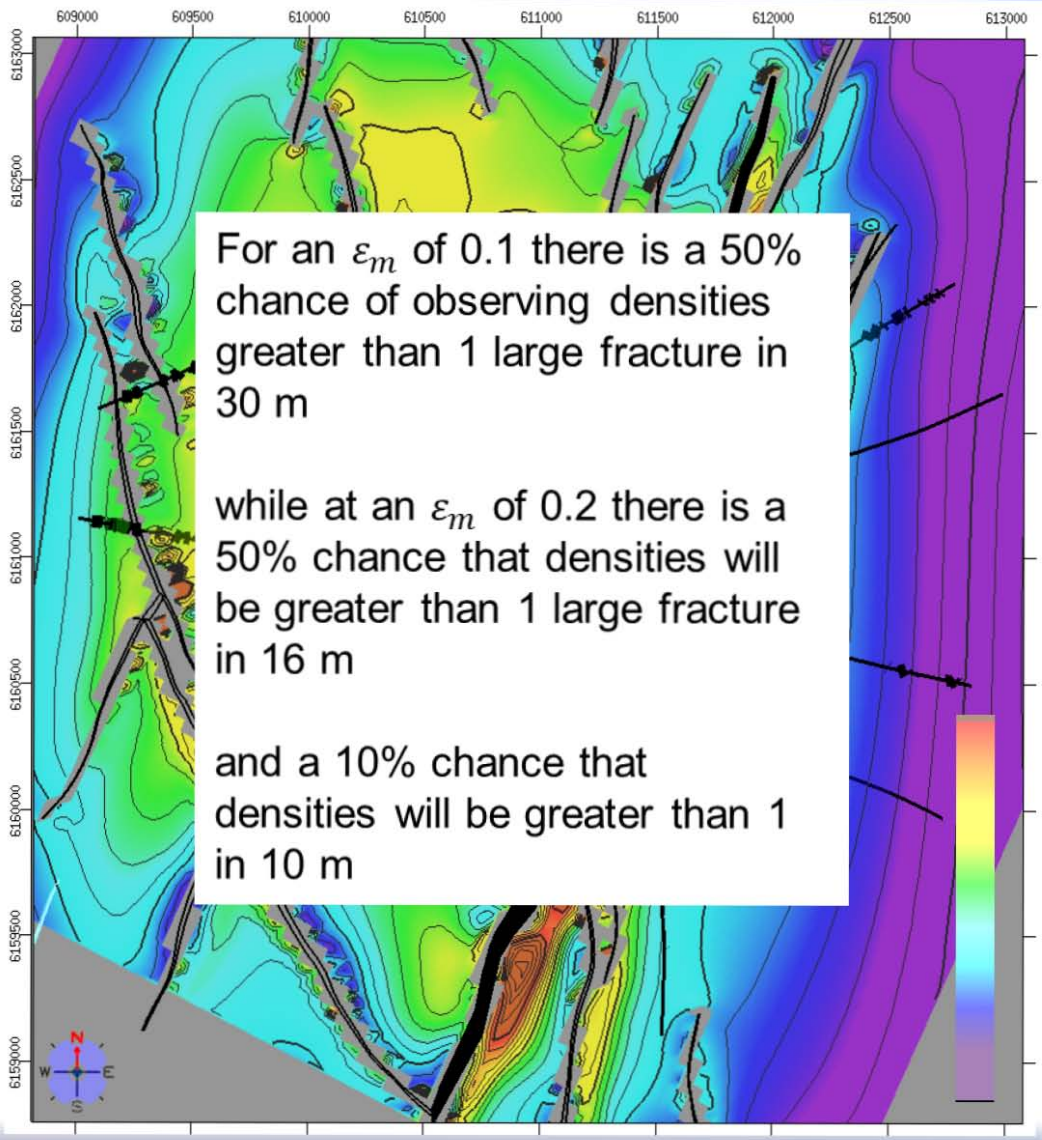

For an ε_m of 0.1 there is a 50% chance of observing densities greater than 1 large fracture in 30 m

while at an ε_m of 0.2 there is a 50% chance that densities will be greater than 1 large fracture in 16 m

and a 10% chance that densities will be greater than 1 in 10 m

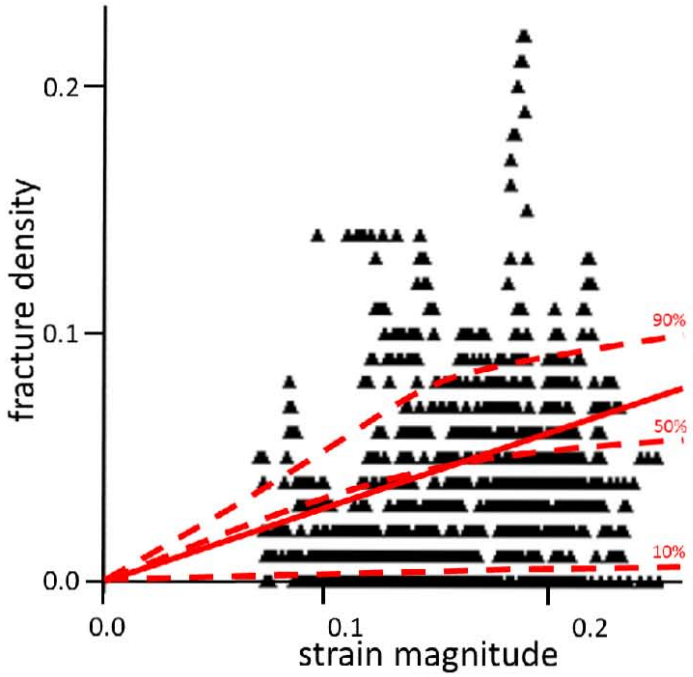

Fracture density calibration, all domains

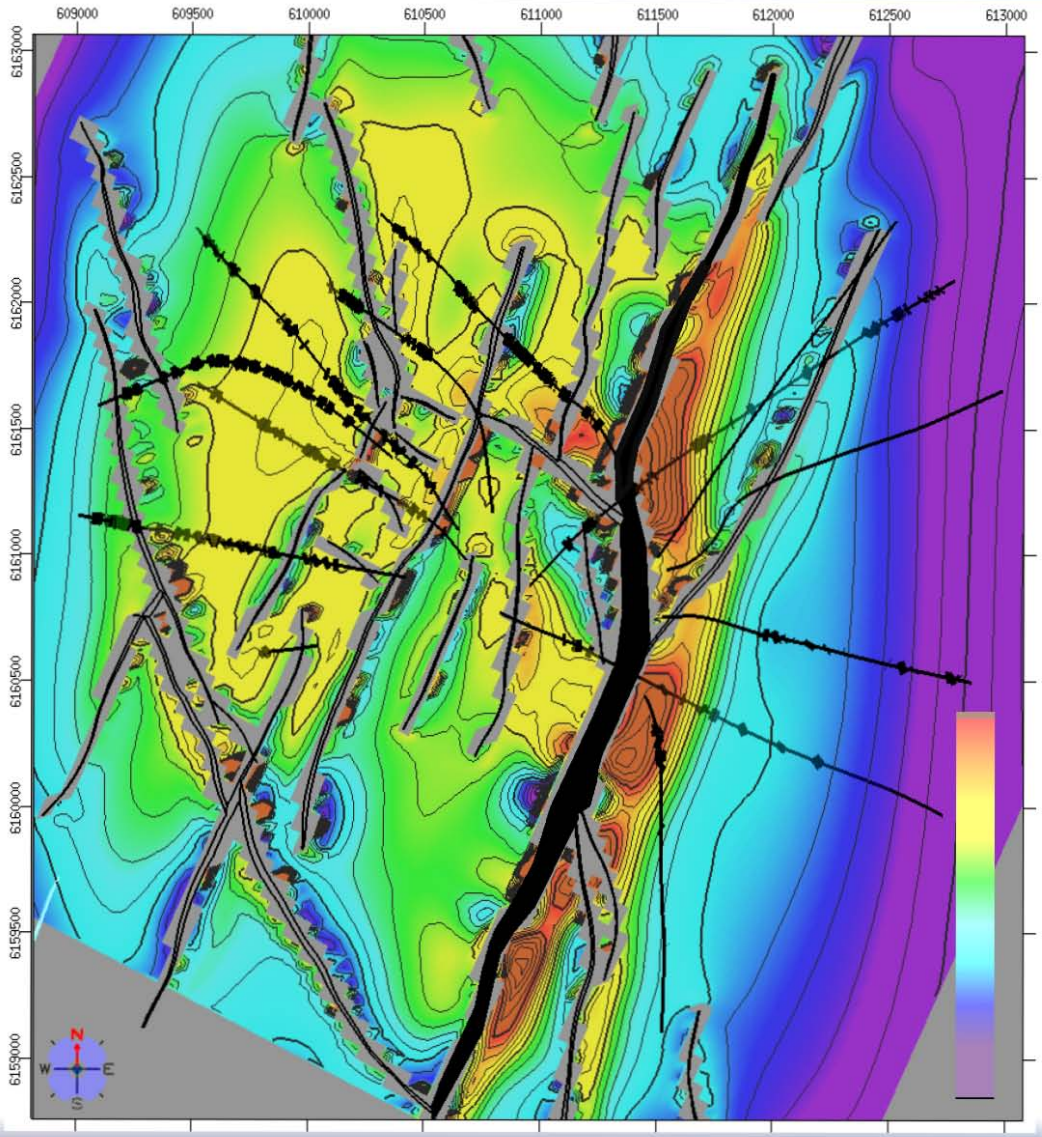

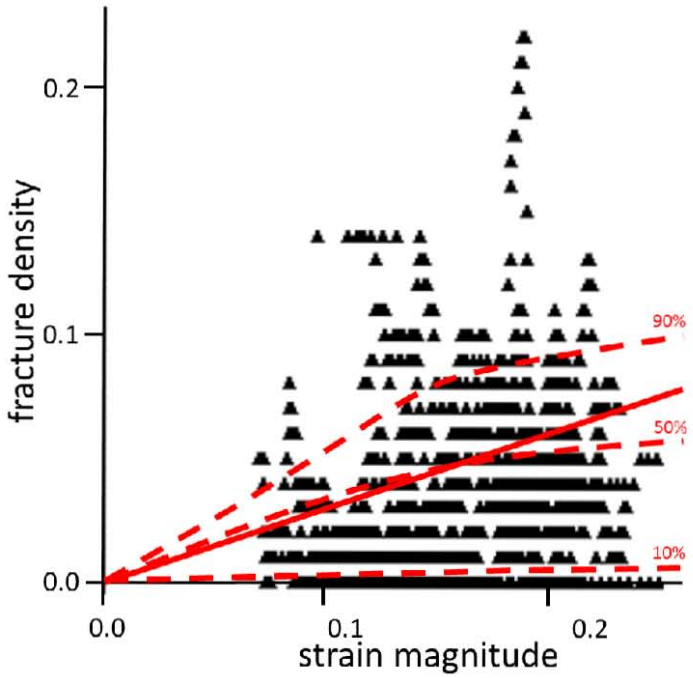

Conclusions

- Strains calculated from an ED model incorporating faults and salt interface as mechanical boundaries correlate with natural fracture orientation and natural fracture density
- Quantitative comparison from 13 wells shows statistically significant correlations between observed and predicted fracture orientations with the median Δp less than 30^{o} and 75% of Δp less than 44^{o}
- Given a broad range of model configurations and other sensitivities the unadulterated geometry derived from the validated mapping is our preferred model
- Our strain magnitude maps correlate with reservoir depletion maps
- Some individual structural domains exhibit nearly linear correlations with observed fracture density – the relationship in some others is less simple
- Collecting data from all domains gives a useful predictive overview showing that the highest observed densities occur at the highest strain magnitudes and that high densities will not be observed at low strain magnitudes